GL00347

UNITED STATES DEPARTMENT OF THE INTERIOR

GEOLOGICAL SURVEY

Fission Track Dating applied to Uranium Mineralization

Erick F. Weiland, Kenneth R. Ludwig,

Charles W. Naeser, and E. Craig Simmons

Denver, Colorado 80225

Open-File Report 80-380

1980

This report is preliminary, and has not been edited or reviewed for

conformity with U.S. Geological Survey standards or nomenclature.

ABSTRACT

The occurrence of quartz adjacent to uraninite in many uranium deposits allows quartz to be employed as a detector to record the spontaneous fission decay of ^{238}U occurring within the adjacent uraninite. A theoretical equation which models the decrease in track density within the quartz with increased distance from the grain boundary with the adjacent uraninite is described in detail. To test this model, quartz grains were placed in a U-solution, irradiated in a reactor to induce ^{235}U fission, and then the track distribution within the quartz determined. The theoretical curves very closely match these data and yield track densities in excellent agreement with the reactor-calculated track density.

Etching experiments on quartz were undertaken to establish values for etching efficiency and etching rates for various crystallographic orientations. Etching efficiency for a plane perpendicular to the c-axis, using KOH-NaOH etching solution at 145°C, has been determined to be 0.38.

To test this model on natural material, samples from the Midnite Mine, Washington were prepared and dated using quartz associated with uraninite; ages of 52 to 54 m.y were obtained. These ages are in excellent agreement with a previously established U-Pb isochron age of 51.0 ± 0.5 m.y.

ACKNOWLEDGEMENTS

INTRODUCTION

To better understand the origin and history of uranium deposits, accurate ages of mineralization are essential. Radiometric age determinations on uranium ores have previously used the U-Pb isotopes (Faure, 1977) and U-series methods (Hamilton and Farquhar, 1968). Discordant results for uranium deposits are commonly obtained by these methods (see Hamilton and Farquhar (1968), Faure (1977), Ludwig (1977), Ludwig and Young (1975) and, Ludwig and others 1977)) because of variance of the mineral system with respect to two basic limiting factors: 1) the closure of the system to loss and gain of the parent and all daughter elements, and 2) lack of sufficiently precise knowledge of the isotopic composition of the initial Pb. Thus a method for determining the age of uranium mineralization involving fewer constraints would be of great value.

The fission-track method of age determination is based upon the fission of ^{238}U atoms into two heavy, highly charged, high velocity fragments. Their passage through most solids creates narrow paths of intense crystal damage on an atomic scale (Fleischer and others, 1975). These damage zones are normally stable in insulating solids over geologic time at low temperatures ($<100^{o}C$) (Naeser, 1976), and may be revealed by use of several techniques, depending on the nature of the solid. A fission-track age is related only to the concentration of ^{238}U, closure of the system to uranium migration, and the stability of tracks. It does not depend upon knowledge of isotopic composition of initial-Pb, or absence of loss or gain of radiogenic-Pb or intermediate decay products. Therefore, fission-track data should yield reliable ages of mineralization for uranium deposits which have been closed to loss or gain of uranium and have remained at temperatures below $100^{o}C$ (to avoid annealing of tracks) since formation.

3

The use of a U-poor mineral phase adjacent to a U-rich phase (where track densities would be too great to resolve) as a register of the fission events is the basis for this research. Previous fission-track dating methods have used the uranium-bearing mineral itself to register the fission events. Here, however, the fission-track density, as a function of distance into the adjacent detector mineral, is used to determine the number of fission events in the uranium bearing phase. Using this method, Haines and others (1975) worked with U-poor phases bordering U-rich whitlockite phases in lunar rocks, and determined ages of formation of lunar samples consistent with those obtained by independent methods.

The registering mineral adjacent to the U-rich mineral to be dated must have a very low uranium concentration, good track registration properties, an ability to reveal well-developed tracks, and a high track annealing temperature. The properties of quartz and its common association with U-rich phases in uranium deposits are the primary reasons for its selection as the detector mineral for this study.

The three main objectives of this investigation were: (1) development of a theoretical model; (2) development of the required techniques and procedures; and (3) application of the method to a uranium deposit.

THEORETICAL MODEL

To represent the decrease in track density in a U-poor phase as a function of distance from the grain boundary with a U-rich phase, a theoretical model based on solid-angle geometry was developed. This model calculates the probability that a fission fragment originating within the U-rich phase will pass through a given unit area on the polished surface within the U-poor phase, and then integrates these probabilities over the volume in the U-rich phase from which a fission fragment may originate and have the required energy

4

to reach the unit area (see detailed discussion in Appendix A). The total probability is given by the integral

$$P_f = \frac{1}{2\pi} \int_{\pi/2}^{\pi} \int_{0}^{2\pi} \int_{0}^{\rho_\ell} \frac{\left| - \rho \sin\phi \cos\theta \cos\alpha + a \cos\alpha \sin\alpha - \rho \cos\alpha \right| \rho^2 \sin\phi \, d\rho \, d\theta \, d\phi}{(a^2 \cos^2\alpha - 2 a \rho \cos\alpha \cos\phi + \rho^2)^{3/2}} \quad (1)$$

Variables are defined in Appendix A and Figure A-1. This integral must be numerically evaluated due to the absolute value within the numerator, and the dependence of the upper limit for the   integration upon the maximum track lengths in the minerals under study. A flow chart, computer program, and generated curves for the numerical evaluation can be found in Appendix A. By plotting track density versus distance from the grain boundary for data from traverses in the detector mineral, and then fitting the theoretical curves to these data, the track density at the grain boundary may be determined. An age (A) may be calculated from this using

$$A = \frac{\rho_s}{(N_v C^{238}) \lambda_F R^{238} n^{238}} \qquad (2)$$

where

ρ_s = spontaneous fission track density in the interior of the U-rich phase.

$N_v C^{238}$ = number of ^{238}U atoms per unit volume (assumed to be uniformly distributed).

λ_F = decay constant for the spontaneous fission of ^{238}U.

R^{238} = range (average travel distance) of fission fragments in the U-rich phase.

5

η^{238} = etching efficiency (defined on page B-1) of fission tracks

in the U-poor phase (detector mineral).

(Naeser, 1976)

The term $N_v C^{238}$ may be estimated by neutron irradiation of the sample in contact with a mica detector, which irradiation induces the ^{235}U to undergo fission (see Naeser, 1976 and Fleischer and others, 1975 for various methods). The induced track density (ρ_i) is then determined within the mica detector for the vein area adjacent to the detector grain to be counted. This allows the age of formation to be calculated using the general fission track age equation:

$$A = \frac{1}{\lambda_D} \ln\left[1 + \frac{\rho_s}{\rho_i}\left(\frac{\lambda_D\,(\phi\,\sigma)\,I}{\lambda_F}\right)\right] \tag{3}$$

where

A = age in years

λ_D = total decay constant for ^{238}U (1.54 x 10^{-10}/yr)

λ_F = decay constant for spontaneous fission of ^{238}U, (7.03 x 10^{-17}/yr)

ϕ = integrated neutron flux from irradiation.

σ = thermal neutron fission cross section for ^{235}U, (582 x 10^{-24}cm^2)

I = atomic ratio of $^{235}U/^{238}U$, (7.26 x 10^{-3})

(Naeser, 1976)

TECHNIQUES AND PROCEDURES

Samples from the Midnite Mine, Washington were selected, as a $^{207}Pb/^{204}Pb-^{235}U/^{204}Pb$ isochron age for these ores of 51.0±0.5 m.y. has been previously established (Ludwig and others, 1978) and the samples

contain the requisite uraninite-quartz relationships. Polished thin sections
of the vein samples were prepared and studied to locate the quartz grains to
be used for age determinations. Since viewing down the c-axis is an easily
recognized orientation in quartz crystals and this orientation produces
consistent etching characteristics (Appendix B), grains with this orientation
were chosen for study. The other considerations in choosing the specific
grain to be used were, first, that little or no uraninite/coffinite
intermixing adjacent to the quartz should be indicated by reflected light
microscopy, and second that the quartz grain be no less than 50 μm in diameter.

A mica detector was then taped to the polished surface over the entire
sample. This package was placed into a reactor tube and irradiated in the U.S
Geological Survey "Lazy Susan" position of the TRIGA research reactor in
Denver. The sample received a thermal neutron dose of 9.45×10^{11}
neutrons/cm^2. The mica detector was then removed from the sample, etched in
HF at 25°C for 14 minutes, and the induced track density counted so that
equation 3 could be used for age calculations.

The Midnite Mine sample was etched in a solution containing 14 g. KOH, 10
g NaOH, and 10 g H$_2$O at 145°C for 3.5 minutes to reveal the fission tracks
(described in detail in Appendix B). Since track densities of 10^9
tracks/cm^2 or greater were expected, counting of tracks required a
transmission electron microscope (TEM). A two stage replication technique,
modified from Kay (1965), was used in preparation of TEM specimens. Briefly,
this technique involves replicating the etched surface with cellulose acetate
softened with acetone. When the acetone has evaporated and the cellulose
acetate re-hardened, the plastic replica is carefully peeled off the surface.
It is generally necessary to do this several times before a satisfactory
replica is obtained. The replica is then shadow-coated with a 20-50 $\overset{o}{A}$ metal

7

layer (Pd or Pt) at 20-30° from the horizontal, and then carbon coated (200-400 Å) perpendicular to the replicated surface in an evaporative coating apparatus. The plastic replica is completely dissolved, leaving the metal-carbon replica which is placed on a TEM grid (see Appendix B for detailed procedure).

The replicated quartz grain, which has been previously selected for counting, is located under low magnification in the TEM. Areas to be counted, chosen according to previously defined criteria, were then photographed. It is necessary that the photomicrographs cover sufficient distance into the interior of the grain to record all tracks originating from the uraninite phase. A photo-mosaic was made from the photomicrograph prints. Track densities at several distances from the grain boundary were then determined from the photomicrographs. Where possible, pooling of the track counts was used to improve the statistics since only tens of tracks per square micron could be counted. The results were plotted and a theoretical curve fitted to the data.

Curves were fitted by determining the grain boundary angle to the nearest 10°, using the maximum distance into the detector mineral at which tracks still appear, and the distance from the grain boundary at which a decrease of one order of magnitude in track density occurs. A correction component in the Y-axis was then added or subtracted to the corresponding theoretical curve until the best apparent visual fit was found. From the intercept of this curve, an age was determined using equation 3.

RESULTS

Three age determinations for the Midnite Mine, made from two quartz grains from sample #MD-256, are presented here.

8

Data from the Midnite Mine sample yield the following results. Sample MD-256-EW-3 (A) has an intercept value of 35.2 tracks/μm^2, based on parallel count traverses (Table 1 and Figure 1). Data from sample MD-256-EW-3 (C), based on 6 parallel count traverses within the same quartz grain as MD-256-EW-3 (A), yields an intercept of 36.3 tracks/μm^2 (Table 1 and Figure 2). Sample MD-256-EW-3 (D), yields an intercept of 35.9 tracks/μm^2 based on 1 traverse only (Table 1 and Figure 3). This sample is from another grain which has coffinite/uraninite intermixing problems, as indicated by subsequent ore-microscope examination, and therefore is not included in the final age calculation. Data from sample #MD-256-EW-3 (B) have not been included here because fission tracks were recorded as far as 35 μm into the quartz grain, suggesting an irregular distribution of uraninite surrounding the quartz and an irregular shape of the quartz grain.

Uncertainties for all counts are based on a Poisson distribution for fission events. The relative standard derivation has been determined by taking the square root of the total number of tracks counted and dividing by the total number of tracks counted. All uncertainties given are $\pm$ 2 standard deviations (2σ).

From the reactor irradiation, the induced track density in the mica detector was calculated to be 1.003×10^7 tracks/cm^2 using

$$\rho_T = \frac{U \phi}{5.76 \times 10^{10}}$$

where

ρ_T = track density at grain boundary

U = uranium concentration in ppm

ϕ = neutron dose in neutrons/cm^2

* believed to have an uncertainty of $\pm$10 percent (2σ)

TABLE 1

Results from traverses on Midnite Mine, Washington quartz grains. Polished surface perpendicular to the C-axis of quartz grain bounded by uraninite. Track density from pooled data from two or more adjacent traverses into the grain interior. Uncertainties shown as $\pm 2\sigma$.

Sample Number	Distance from Grain Boundary to Center of Area Counted (microns)	Track Density (tracks/μm^2)	Calculated Track Density at Grain Boundary (tracks/μm^2)	Calculated Age (M.Y.)
MD-256-EW-3 (A)	0.63 ± 0.10	12.82 ± 2.56		
	1.25 ± 0.10	11.28 ± 2.40		
	1.88 ± 0.10	14.87 ± 2.76		
	2.50 ± 0.10	11.79 ± 2.49		
	3.13 ± 0.10	8.72 ± 2.11		
	3.75 ± 0.10	6.67 ± 1.85		
	4.38 ± 0.10	5.64 ± 1.70		
	5.00 ± 0.10	3.08 ± 1.26	35.2	52.8
MD-256-EW-3 (C)	0.63 ± 0.10	6.84 ± 3.40		
	1.25 ± 0.10	8.53 ± 3.80		
	1.88 ± 0.10	14.34 ± 5.40		
	2.50 ± 0.10	9.22 ± 4.40		
	3.13 ± 0.10	13.31 ± 5.20		
	3.75 ± 0.10	7.17 ± 3.80		
	4.38 ± 0.10	4.10 ± 2.90		
	5.00 ± 0.10	3.58 ± 2.70	36.3	54.2
MD-256-EW-3 (D)	1.00 ± 0.10	19.00 ± 4.40		
	2.00 ± 0.10	8.00 ± 2.80		
	3.00 ± 0.10	14.00 ± 3.70		
	4.00 ± 0.10	8.00 ± 2.80		
	5.00 ± 0.10	7.00 ± 2.70		
	6.00 ± 0.10	4.00 ± 2.00		
	7.00 ± 0.10	3.00 ± 1.70	35.9	53.8

MIDNITE MINE SAMPLE

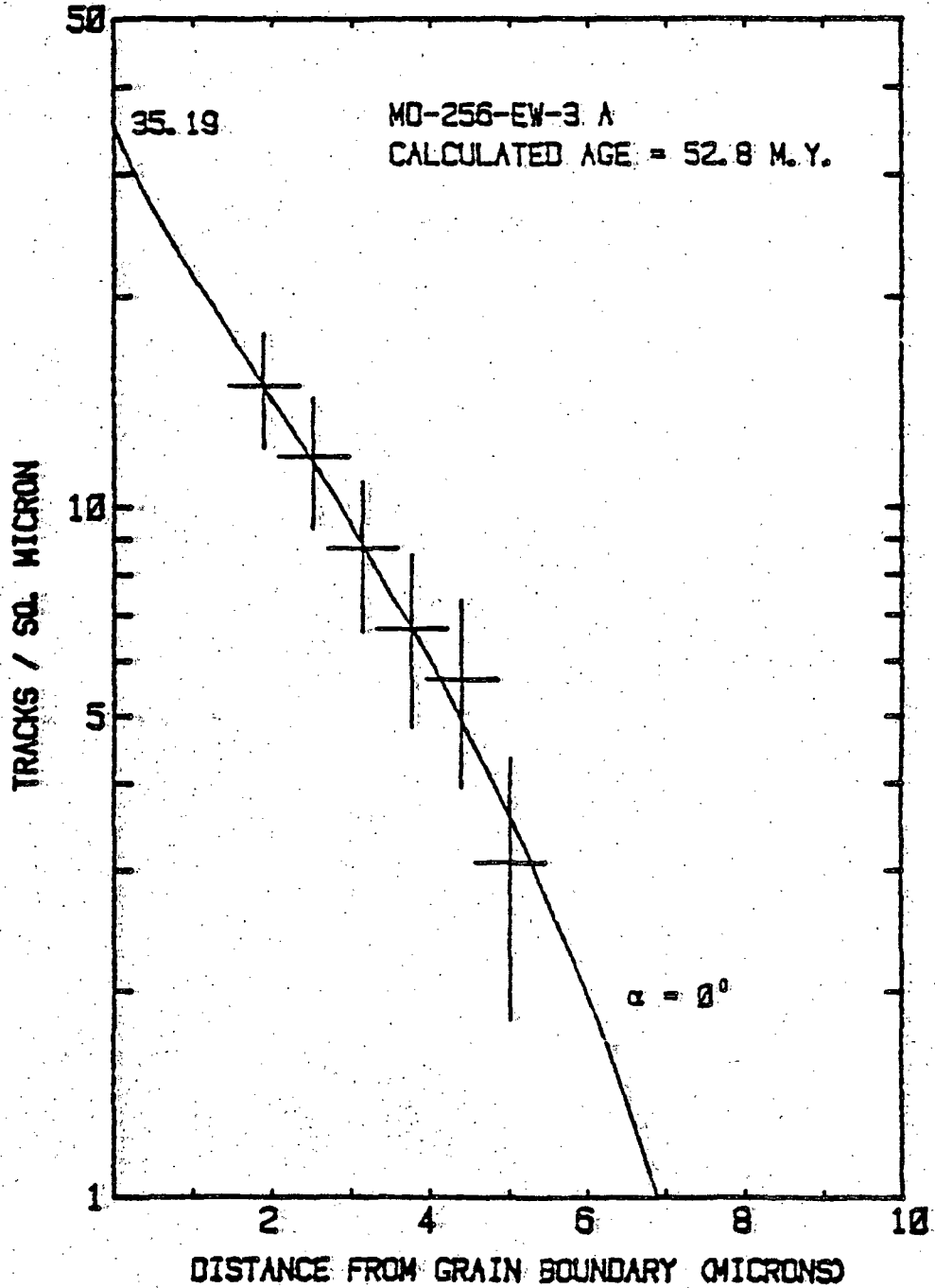Figure 1. A plot of tracks/μm^2 versus distance from the grain boundary to determine the age of mineralization for the Midnite Mine uranium deposit (Washington); α = grain boundary angle.

MIDNITE MINE SAMPLE

Figure 2. A plot of tracks/μm^2 versus distance from the grain boundary to determine the age of mineralization for the Midnite Mine uranium deposit (Washington); α = grain boundary angle.
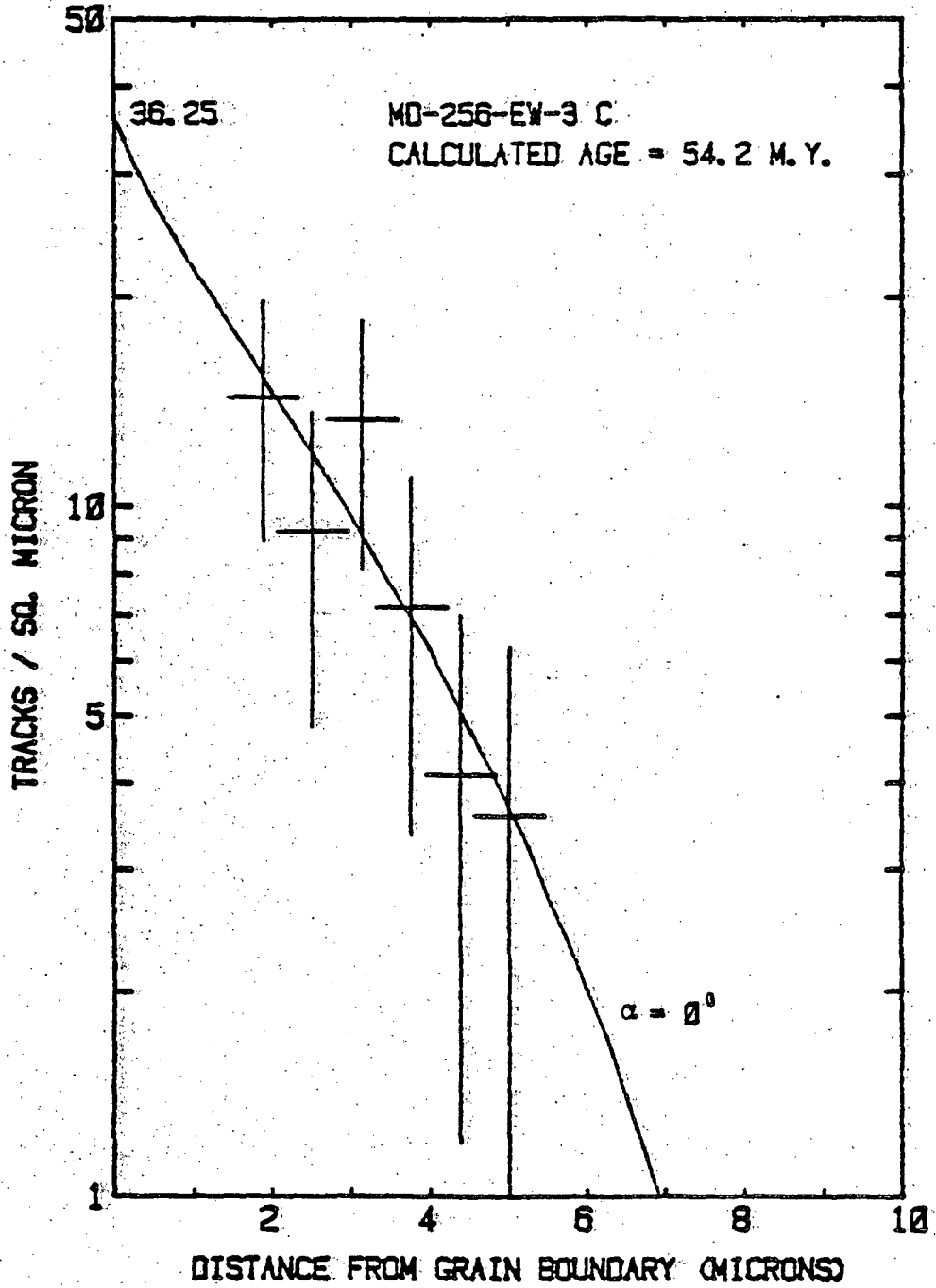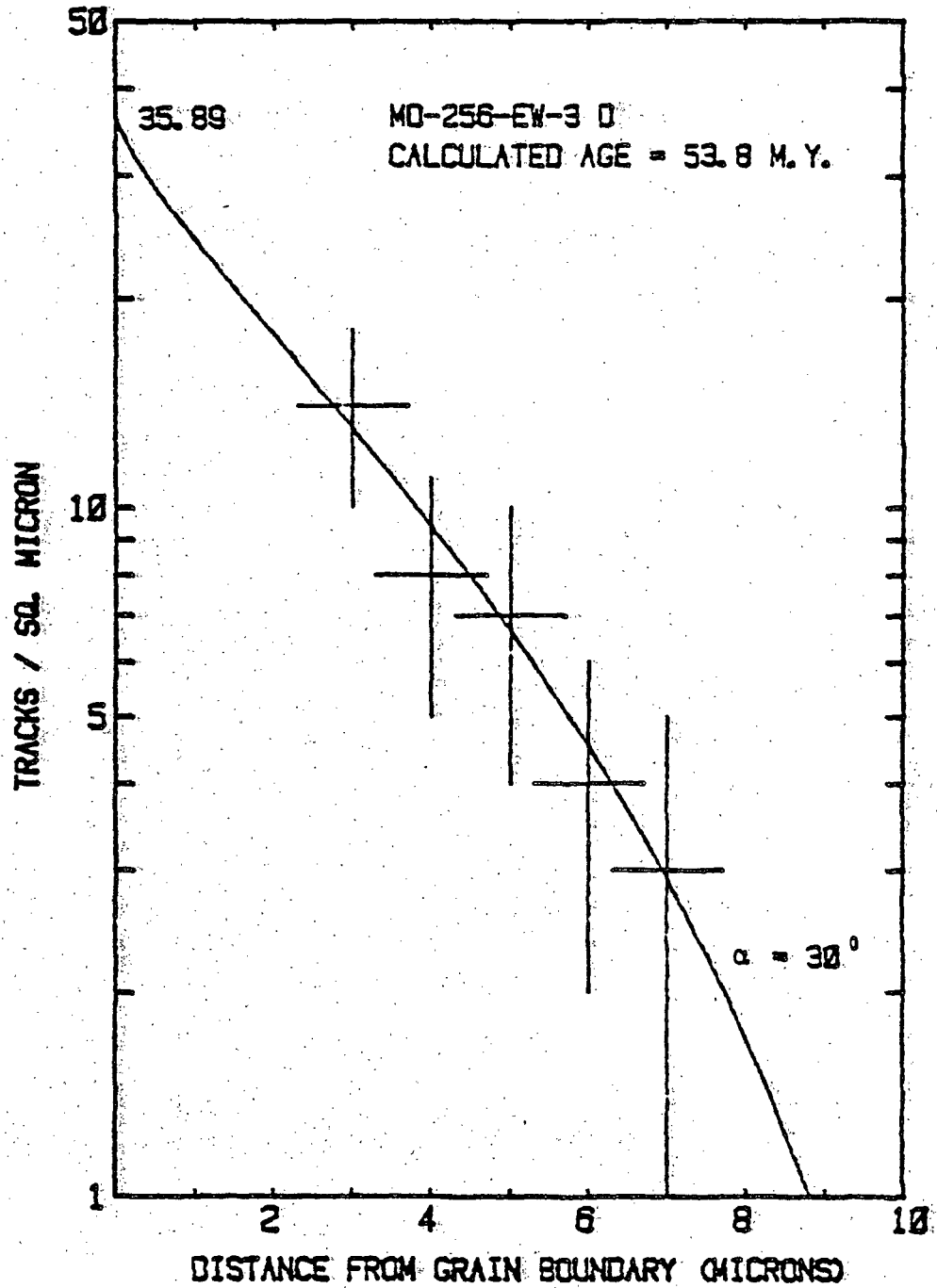
MIDNITE MINE SAMPLE

Figure 3. A plot of tracks/μm^2 versus distance from the grain boundary to determine the age of mineralization for the Midnite Mine uranium deposit (Washington); α = grain boundary angle.

The etching efficiency (n^{238}) in quartz for a polished surface perpendicular to the C-axis is estimated to be 0.38 (Appendix B) and the sample intercepts were multiplied by the reciprocal of n^{238} to calculate the number of fission fragments which passed through the grain boundary. Then using equation 3, the following ages of formation were determined:

Sample	Age (m.y.)
MD-256-EW-3 (A)	52.8
MD-256-EWO3 (C)	54.2
MD-256-EW-3 (D)	53.8

By combining results from MD-256-EW-3 A and C, an age of 53.5 m.y. is given by this fission-track dating method, which is in excellent agreement with the age of 51.0 $\pm$ 0.5 m.y. obtained by Ludwig and others (1978) using the U-Pb method. Uncertainties within the calculated ages cannot presently be determined due to the lack of knowledge of the uncertainties for many of the variables such as n^{238}, R^{238}, and $N_v C^{238}$. However, the data from the reactor irradiated quartz samples (Appendix B) indicate a variation of about ± 10 percent in the calculated track density from the reactor calculated track density.

CONCLUSIONS

The agreement of the fission-track age with the U-Pb isochron age of this natural sample of known age and the results of the reactor-irradiated quartz standards (Appendix B), indicate this fission track technique to be a useful method for dating uranium mineralization. Two critical areas, however, need further investigation. The distance that a fission fragment will travel

through crystal lattices and the fragment's loss of energy over the damage zone must be better understood to obtain accurate track lengths. This is essential for precise numerical evaluation of the theoretical model. The etching efficiency (η^{238}) of the detector mineral is the second area of major concern. Because very few minerals will reveal all the damage zones after etching (Fleischer and others, 1975), determination of the percentage of tracks that will be counted for the number of damage zones actually present is necessary. This will generally change for the various minerals as well as their different cyrstallographic orientations.

For fission track techiques to yield reliable results, the system must have remained closed to loss or gain of U, but not necessarily to the daughter products from the decay of ^{235}U and ^{238}U; quartz must be found adjacent in uraninite or coffinite, with uniform composition of uraninite or coffinite and the correct orientation of quartz desirable; and no thermal event can have occurred where annealing of the damage zones in quartz could have taken place after mineralization.

This fission track dating method should be useful for dating uranium mineralization in an age range of about 10 to 500 m.y., using uraninite adjacent to a quartz detector. This range is based on the expected number of spontaneous fission events naturally occurring in the uraninite, and on the resolution of the etched tracks viewed on the TEM. The method might be extended, however, to older events by use of other U-bearing mineral, such as zircon, sphene, and apatite, where the useful age range will be dependent upon the U-concentration and scale of U-zonation within the mineral chosen.

REFERENCES CITED

Chadderton, L. T., and Torrens, I. McC., 1969, Fission damage in crystals: London, Methuen and Co. p. 1-28.

Faure, G., 1977, Principles of isotope geology: New York, John Wiley and Sons, 464 p.

Fleischer, R. L., and Price, P. B., 1964, Techniques for geological dating of minerals by chemical etching of fission fragment tracks: General Electric Research Laboratory Report no. 64-RL-3635M, 21 p.

Fleischer, R. L., and Price, P. B., 1964, Techniques for geological dating of minerals by chemical etching of fission fragment tracks: Geochim. et Cosmochim. Acta v. 28, p. 1705-1714.

Fleischer, R. L., Price, P. B., and Walker, R. M., 1975, Nuclear trakcs in solids, principles and applications: Berkeley, University of California Press, 605 p.

Friedlander, G., Kennedy, J. W., Miller, J. M., 1964, Nuclear and radio-chemistry: New York, John Wiley and Sons, 2nd ed., p. 86-103.

Frondel, C., 1962, Dana's sytem of mineralogy: New York, John Wiley and Sons, p. 36-60.

Haines, E. L., Hutcheon, I. D., and Weiss, J. R., 1975, The fission track record of Apennine Front KREEP basalts: Proceedings, Lunar Science Conference 6, p. 3527-3540.

Hamilton, E. I., and Farquhar, R. M., 1968, Radiometric dating for geologists: New York, John Wiley and Sons.

Kay, D. H., 1965, Techniques for electron microscopy: Great Britain, Blackwell Scientific Publications LTD., p. 96-151.

Ludwig, K. R., 1977, Effect of initial radioactive-daughter disequilibrium on U-Pb isotope apparent ages on young minerals: U. S. Geological Survey, Journal Research, v. 5, no. 6, p. 663-667.

Ludwig, K. R., Naeser, C. R., and Nash, J. T., 1978, Uranium-lead ages of
uranium ores from the Midnite Mine, Washington (abs.) Economic Geology, v.
73, no. 7, p. 1393.

Ludwig, K. R., Szabo, B. J., Granger, H. C., 1977, Pleistocene apparent ores by
U-Pb isotope and U-series methods for uranium ore in Dakota Sandstone near
Gallup, New Mexico: U.S. Geological Survey, Journal Research, v. 5, no.
6, p. 669-672.

Ludwig, K. R., and Young, E. J., 1975, Absolute age of disseminated uraninite
in Wheeler Basin, Grand County, Colorado: U. S. Geological Survey,
Journal Research v. 3, no. 6, p. 747-751.

Naeser, C. W., 1976, Fission track dating: U.S. Geological Survey Open-File
Report 76-190, 66 p.

Protter, M. H., and Morrey, C. B., Jr., 1964, College calculus with analytic
geometry: Palo Alto, Addison-Wesley, 527 p.

Sowinski, M., Stéphan, C., Czyzewski, T., and Tys, J., 1972, Le quartz
cristallin detecteur de traces de particules lourdes chargées: Nuclear
Instruments and Methods, no. 105, p. 317-322, (in French).

APPENDIX A - Derivation of the theoretical distribution of track density as a
function of distance from the grain boundary on a polished surface.

To understand how the track density within a U-poor phase varies with
distance from the grain boundary with a U-rich phase, the following
mathematical model is proposed. This model uses solid angle geometry to
determine the probability that a fission fragment originating within the
U-rich phase will pass through a given unit area on the polished surface
within the U-poor phase. By integrating over the volume in the U-rich phase
from which a fission fragment may originate and pass through the unit area at
a specific distance from the grain boundary, the total probability for all
fission fragments may be calculated for the unit area. Figure A-1 illustrates
the geometrical relationships and requisite parameters in setting up the
integrand.

DEFINITIONS (See also Figure A-1):

P_f is the total probability that any fission fragment from the U-rich
phase may pass through the unit area on the polished surface.

P_i is the probability that a fission fragment originating within a
differential volume will pass through the unit area.

$\vec{P}$ is the unit vector from the differential volume dV to the center of the
unit area.

R is the distance from the differential volume dV to the center of the
unit area.

$\vec{d}$ is the unit vector normal to the unit area a distance "a" from the grain
boundary on the polished surface.

d' is the distance from the origin to the center of the unit area.

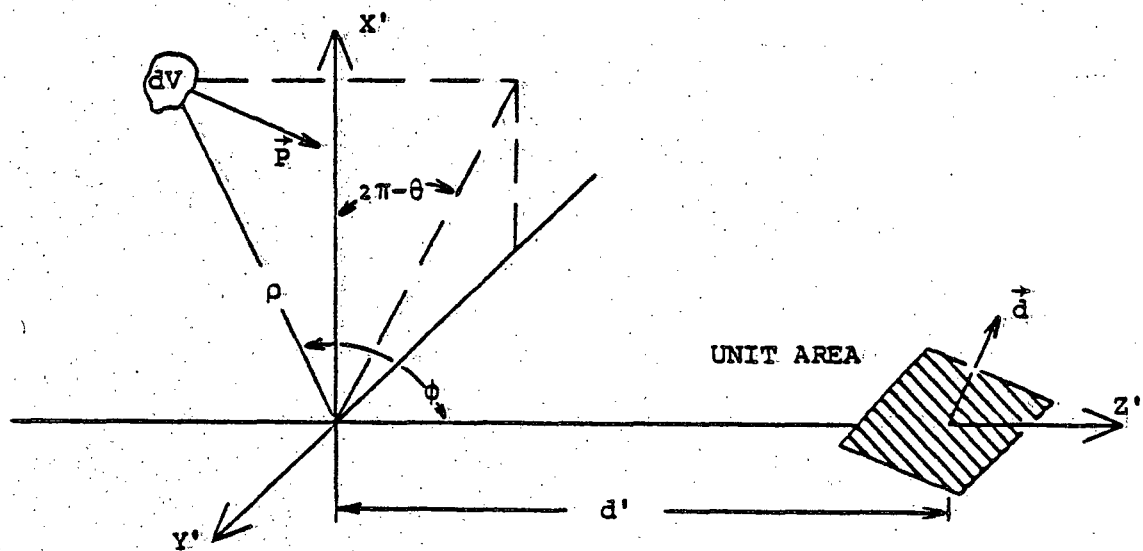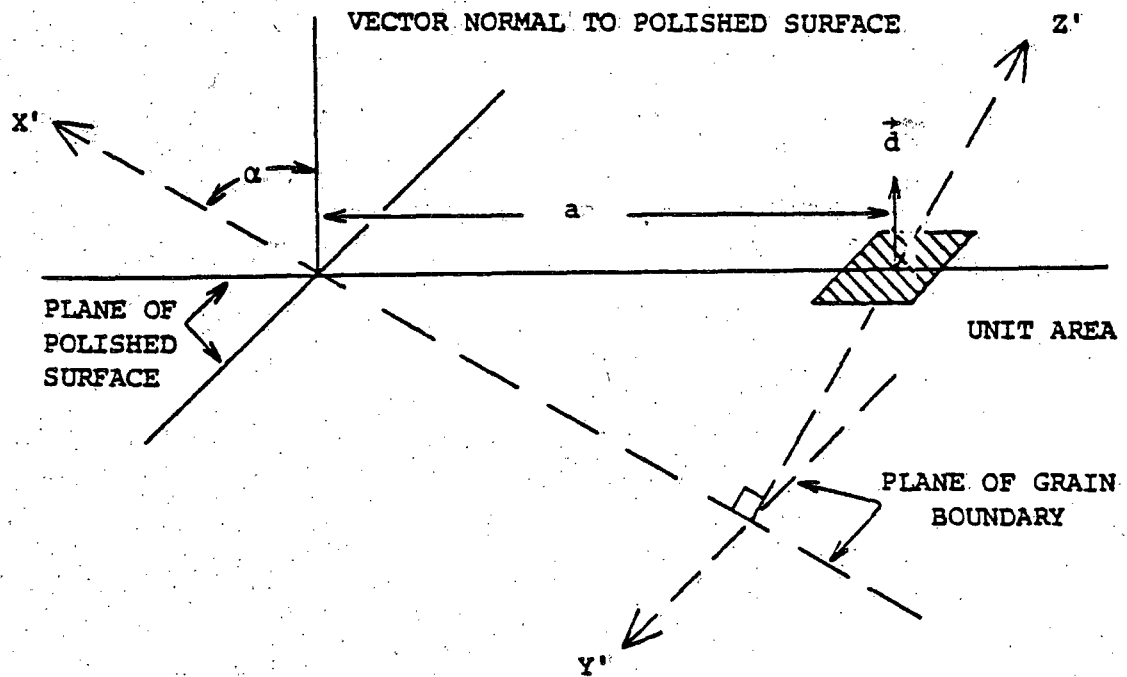is the vector from the origin to the differential volume dV.

A-1

Figure A-1. The geometrical relationships and requisite parameters for setting up the theoretical model are illustrated in these diagrams.

α is the angle measured from the normal vector to the polished surface to the grain boundary.

ϕ is the angle measured from the positive Z axis to the vector .

θ is the angle measured counterclockwise from the positive X axis to the projection of the vector on the X-Y plane.

dE/dD is the energy loss (dE) of a fission fragment divided by the distance traveled (dD) through a substance during the energy loss.

The following equalities hold for a spherical coordinate system where i, j, and k are unit vectors parallel to the respective axes X, Y, Z:

$$\vec{d} = \cos\alpha\,\vec{i} + \sin\alpha\,\vec{j}$$

$$R = \{(-\rho\sin\phi\cos\theta)^2 + (-\rho\sin\phi\sin\theta)^2 + (a\cos\alpha - \rho\cos\theta)^2\}^{1/2}$$

$$\vec{P} = \frac{(-\rho\sin\phi\cos\theta)\vec{i} + (-\rho\sin\phi\sin\theta)\vec{j} + (a\cos\alpha - \rho\cos\theta)\vec{k}}{R}$$

$$d' = a\cos\alpha$$

DERIVATION OF THE PROBABILITY FUNCTION

The probability that any one fission fragment from the differential volume (dV) will pass through the unit area is given by the solid angle subtended by the projection of the unit area on a sphere divided by the total solid angle (4π steradians) of the sphere, modified for the case of fissioning ^{238}U atoms since two particles are produced in each fission event. Since, for the geometrical relationships given in Figure A-1, the area of the projection of the unit area onto a sphere of radius R is $(\vec{P}\cdot\vec{d})$, then P_i, the probability that one of the two fission fragments originating in dV will pass through the unit area is:

$$P_i = \frac{|\vec{P}\cdot\vec{d}|}{2\pi R^2}$$

To determine the probability (P) of all fission fragments which may pass through the unit area, P_i is integrated over the volume from which a fission fragment may originate within the U-rich phase and have sufficient energy to reach the unit area. Substituting in the required quantities and simplifying the denominator by squaring terms and using the trigometric equaltiy.

$$1 = \sin^2 a + \cos^2 a$$

yields the following equation:

$$P_f = \frac{1}{2\pi} \int_V \frac{|\cos \alpha \, (- \alpha \sin \phi \cos \theta) + \sin \alpha \, (a \cos \alpha - \rho \cos \phi)| \rho^2 \sin \phi \, d\rho \, d\theta \, d\phi}{(a^2 \cos^2 \alpha - 2 \, a \, \rho \cos \alpha \cos \phi + \rho^2)^{3/2}}$$

LIMITS OF INTEGRATION

Due to the semi-spherical nature of the volume from which a fission fragment may originate (Figure A-2), the limits of integration for the integral will be 0 to 2π. Because fission fragments do not originate within the U-poor phase, the lower limit for the θ integration will be $\pi/2$. The upper limit for ϕ will be π since angles greater than this would only duplicate the volume already accounted for within the θ integration.

The lower limit for the ρ integration will be zero because fission fragments only originate within the U-rich phase. The upper limit of integration $(\rho\ell)$ however, depends upon the maximum distance a fission particle will travel through the mineral phases. Close inspection indicates that $\rho\ell$ is
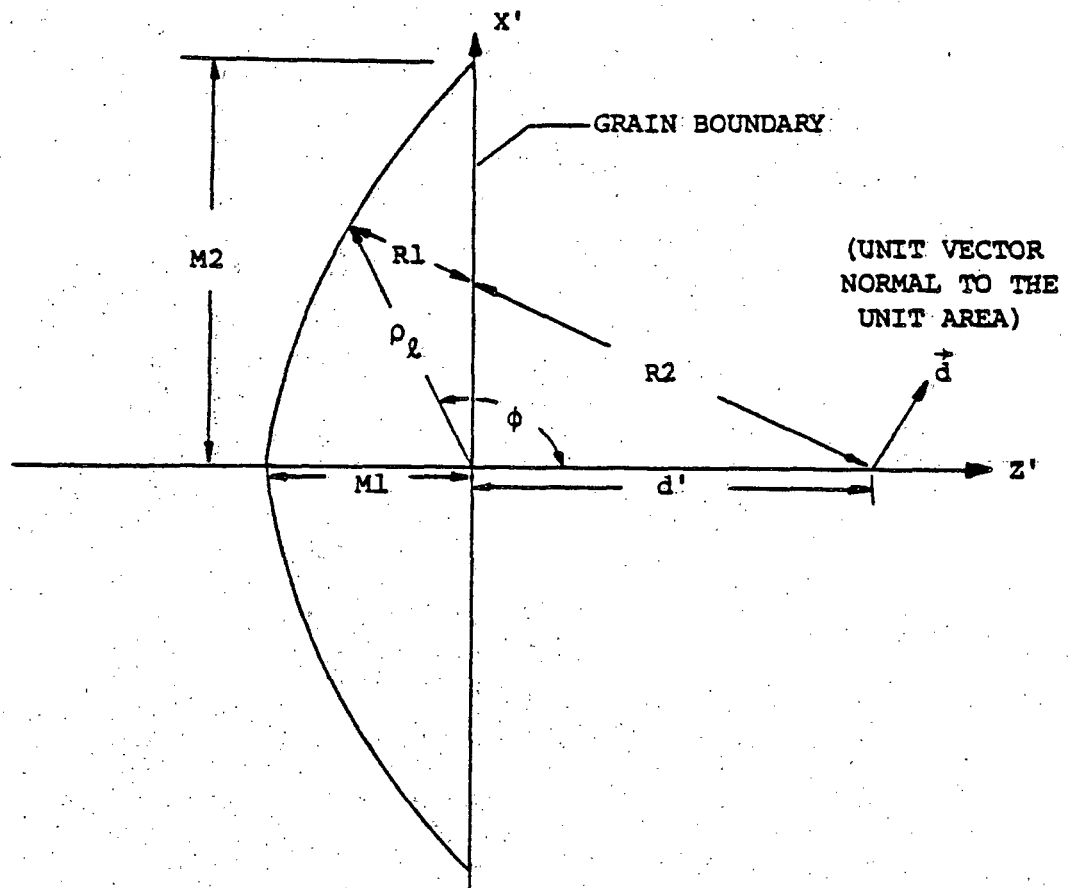
Figure A-2. Two dimensional diagram illustrating quantities required to determine the upper limit for the ρ integration.

therefore dependent upon the angle φ but not on the angle θ, again due to the semi-spherical shape (Figure A-2). The total energy loss $\int (dE/dD)$ of the fission fragment will be equal to the sum of the energy loss in phases "a" and "b",

$$\int \frac{dE}{dD} = \left[\frac{dE}{dD} \right]_a + \left[\frac{dE}{dD} \right]_b$$

by conservation of energy. Because the energy loss in each mineral is directly proportional to the distance traveled in that mineral, if this loss is assumed to be a linear relationship, then the sum of the ratios of the distance traveled (R) to the maximum track length (M) is each mineral will be equal to unity for total fragment travel. The energy loss is not actually a linear function of the distance traveled (Friedlander and others, 1964), but the assumption will allow a first order approximation of fragment travel distance especially in materials where energy loss curves are not available. Therefore, the fragment will reach the unit area if:

$$\frac{Ra}{Ma} + \frac{Rb}{Mb} \geqq 1 .$$

The maximum limit of integration for ρ is determined when this equality equals unity since this would be farthest point within the U-rich phase from which a fragment could originate and still just reach the unit area. Because the value of $\rho\ell$ is dependent on the angle ϕ and the distance d', the value is best determined within the ϕ integration by some iteration technique. This can be done when ϕ and d' are known by calculating

$$Rb = d' \frac{2 L d'}{L^2 + d'^2 - \rho^2}$$

where

$$L = (\rho^2 + d'^2 - 2 \rho d' \cos \phi)^{1/2}$$

and

$$Ra = L - Rb.$$

When

$$\frac{Ra}{Ma} + \frac{Rb}{Mb} = 1$$

the value used for ρ equals $\rho\ell$. Because the ρ integration is not dependent upon the θ integration, the ρ integration is best evaluated within the θ integration.

The integration to be evaluated is:

$$\Gamma = \frac{1}{2\pi} \int_{\pi/2}^{\pi} \int_{0}^{2\pi} \int_{0}^{\rho_\ell} \frac{|-\rho \sin \phi \cos \theta \cos \alpha + a \cos \alpha \sin \alpha - \rho \cos \phi \sin \alpha| \rho^2 \sin \phi \, d\rho \, d\theta \, d\phi}{(a^2 \cos^2 \alpha - 2 a \rho \cos \alpha \cos \phi + \rho^2)^{3/2}}$$

This integral is not easily solved exactly due to the absolute value within

the numerator and must therefore be solved numerically, using an approach

involving Simpson's approximation.   Simpson's rule states:

"Suppose that $f(x)$ is continuous for $a \leq x \leq b$ and
$\{a = x_0 < x_1 < x_2 < \cdots < x_{2n-1} < x_{2n} = b\}$ is a sub-
division of $[a,b]$ into 2n intervals of length
$h = (b-a)/2n$. Then, approximately

$$\int_a^b f(x)\ dx = \frac{h}{3}\left[f(x_0) + 4f(x_1) + 2f(x_2) + \cdots + 4f(x_{2n-1}) + f(x_{2n})\right]\ "$$

(from Protter and Morrey, 1967).

The computation is further complicated since the maximum distance a fission

fragment may travel within a crystal lattice varies from mineral to mineral.

Figure A-3 and Table A-1 show presently available data on track lengths for

several materials.   Thus $\rho\ell$ must be determined during numerical integration as

described earlier.   Figure A-4 shows the computer program, and table A-3

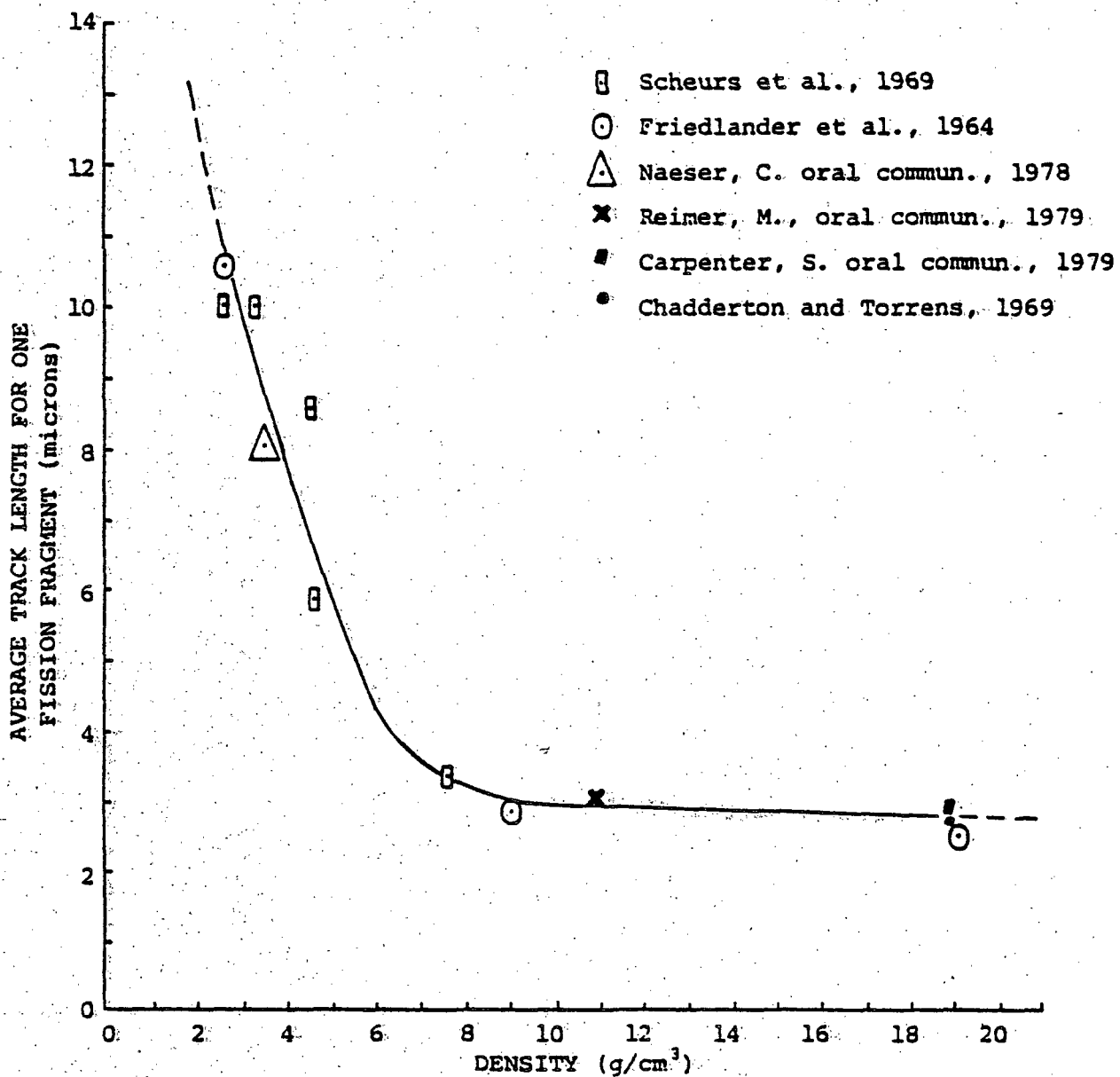list the tabulated values from the numerical evaluation of the integral.

Figure A-3. Average fission fragment travel as a function of density. Since reliable values for tracks lengths are difficult to ascertain, uncertainties for this data have not been established.

TABLE A-1

The average distance a fission fragment will travel in various materials.

Material	Track Length	Reference
Air (STP)	17.0 cm 15.0 cm	Friedlander and others, 1964 Chadderton & Torrens, 1969
Quartz	10.0 μm	Weiland experimental data
Apatite	8.0 μm	Naeser, oral comm., 1978
$MgSiO_3$	10.0 μm	Schreurs, unpub. data, 1969
$FeSiO_3$	8.5 μm	Schreurs, unpub. data, 1969
MgS_2	5.8 μm	Schreurs, unpub. data, 1969
PbS	3.3 μm	Schreurs, unpub. data, 1969
Ni (metal)	2.8 μm	Friedlander and others, 1964 (Figure 4-6)
Au (metal)	2.5 μm	Friedlander and others, 1964 (Figure 4-6)
U (metal)	3.0 μm 2.8 μm	Carpenter, oral comm., 1979 Chadderton & Torrens, 1969
UO_2	3.0 μm	Reimer, oral comm., 1979

TABLE A-2

Values of P_r from the numerical evaluation of the theoretical
model. The P_r integral was evaluated using Simpson's Rule with
a step size (2n) equal to 22. These values are for an average
Maximum fission fragment travel of 10 microns in uraninite and
10 microns in quartz.

Distance from Grain Boundary to Unit Area (microns)	Angle from the Grain Boundary to the Perpendicular of the Polished Surface						
	0^δ	10^δ	20^δ	30^δ	40^δ	50^δ	60^δ
0.0	4.85	4.85	4.85	4.85	4.85	4.85	4.85
0.5	3.77	3.85	3.94	4.06	4.21	4.40	4.53
1.0	3.04	3.13	3.25	3.44	3.67	3.96	4.25
1.5	2.49	2.57	2.72	2.94	3.22	3.59	3.98
2.0	2.03	2.12	2.27	2.52	2.84	3.26	3.71
2.5	1.65	1.74	1.90	2.17	2.51	2.97	3.47
3.0	1.34	1.42	1.58	1.86	2.22	2.70	3.24
3.5	1.08	1.15	1.31	1.58	1.95	2.45	3.03
4.0	0.853	0.920	1.07	1.35	1.72	2.23	2.83
4.5	0.666	0.727	0.874	1.14	1.50	2.02	2.64
5.0	0.511	0.566	0.702	0.952	1.31	1.83	2.46
5.5	0.383	0.409	0.555	0.790	1.13	1.65	2.29
6.0	0.278	0.319	0.432	0.647	0.977	1.48	2.13
6.5	0.195	0.229	0.328	0.524	0.834	1.32	1.98
7.0	0.130	0.158	0.242	0.416	0.705	1.18	1.83
7.5	0.081	0.103	0.172	0.325	0.589	1.04	1.69
8.0	0.045	0.061	0.117	0.247	0.485	0.914	1.56
8.5	0.022	0.033	0.074	0.180	0.393	0.796	1.43
9.0	0.008	0.014	0.042	0.125	0.310	0.688	1.31
9.5	0.001	0.004	0.020	0.080	0.239	0.587	1.19
10.0			0.006	0.046	0.176	0.469	1.08
10.5				0.021	0.123	0.410	0.977
11.0				0.006	0.080	0.333	0.877
11.5					0.046	0.267	0.782
12.0					0.021	0.203	0.693
12.5					0.011	0.151	0.609
13.0						0.105	0.530
13.5						0.068	0.457
14.0						0.040	0.390
14.5						0.019	0.327
15.0						0.005	0.271
15.5							0.219
16.0							0.173
16.5							0.133
17.0							0.098
17.5							0.068
18.0							0.043
18.5							0.025
19.0							0.011
19.5							0.003

TABLE A-3

Values of P_r from the numerical evaluation of the theoretical model. The P_r integral was evaluated using Simpson's Rule with a step size $(2n)$ equal to 22. These values are for an average maximum fission fragment travel of 3 microns in uraninite and 10 microns in quartz.

Distance from Grain Boundary to Unit Area (microns)	Angle from the Grain Boundary to the Perpendicular of the Polished Surface						
	0°	10°	20°	30°	40°	50°	60°
0.0	1.56	1.56	1.56	1.56	1.56	1.56	1.56
0.5	1.18	1.19	1.22	1.25	1.30	1.35	1.41
1.0	0.942	0.962	1.00	1.05	1.13	1.21	1.30
1.5	0.769	0.787	0.831	0.899	0.991	1.10	1.21
2.0	0.627	0.649	0.693	0.772	0.874	0.990	1.13
2.5	0.513	0.530	0.579	0.659	0.773	0.902	1.05
3.0	0.415	0.430	0.482	0.565	0.685	0.822	0.985
3.5	0.330	0.349	0.399	0.484	0.599	0.746	0.922
4.0	0.266	0.281	0.329	0.408	0.527	0.646	0.861
4.5	0.205	0.222	0.267	0.346	0.462	0.619	0.805
5.0	0.159	0.172	0.216	0.289	0.402	0.558	0.751
5.5	0.118	0.131	0.170	0.239	0.350	0.498	0.700
6.0	0.087	0.098	0.133	0.198	0.302	0.449	0.649
6.5	0.060	0.070	0.101	0.159	0.256	0.401	0.602
7.0	0.041	0.049	0.074	0.127	0.219	0.357	0.600
7.5	0.026	0.032	0.054	0.098	0.184	0.315	0.517
8.0	0.014	0.019	0.036	0.074	0.149	0.276	0.474
8.5	0.007	0.010	0.023	0.054	0.122	0.241	0.437
9.0	0.003	0.005	0.013	0.037	0.097	0.207	0.401
9.5		0.001	0.006	0.025	0.074	0.178	0.363
10.0			0.002	0.014	0.055	0.150	0.330
10.5				0.007	0.039	0.124	0.299
11.0				0.002	0.025	0.101	0.269
11.5					0.015	0.081	0.240
12.0					0.007	0.062	0.212
12.5					0.002	0.046	0.186
13.0						0.032	0.162
13.5						0.021	0.140
14.0						0.012	0.119
14.5						0.006	0.101
15.0						0.002	0.083
15.5							0.068
16.0							0.054
16.5							0.041
17.0							0.031
17.5							0.021
18.0							0.014
18.5							0.008
19.0							0.004
19.5							0.001

Figure A-4. Computer program to numerically
evaluate theoretical model using Simpson's
Approximation.

```
10 COM S[100],TS[100],A
20 MAT S=ZER
30 MAT T=ZER
40 RAD
50 REM WEILAND FISSION TRACK DISTRIBUTION CALCULATION
60 DIM X[50],Y[50],Z[50]
70 REM INITIALIZE ALL REQUIRED QUANTITIES
80 DISP "ANGLE BETWEEN NORMAL TO POLISHED SURFACE AND GRAIN BOUNDARY";
90 INPUT A
100 DISP "STEP SIZE FOR LIMIT RHO INTEGRAL";
110 INPUT M2
120 DISP "STEP INTERVAL FOR INTEGRATION";
130 INPUT N
140 DISP "MAX FRAGMENT TRAVEL IN URANINITE";
150 INPUT U
160 DISP "MAX FRAGMENT TRAVEL IN QTZ";
170 INPUT Q
180 DISP "DISTANCE INTERVAL";
190 INPUT DO
200 D=DO
210 REM DETERMINE MINERAL WITH MAX FRAGMENT TRAVEL DISTANCE TO
220 REM DETERMINE LIMIT ON THE RHO INTEGRATION
230 IF U<Q THEN 260
240 M1=U
250 GOTO 280
260 M1=Q
270 REM DETERMINE STEP SIZE FOR THETA AND PHI INTEGRATIONS
280 H1=PI/N
290 H2=PI/(4*N)
300 REM PRINT DATA HEADINGS FOR OUTPUT FROM PROGRAM
310 PRINT LIN1 "TRACK LENGTH GRANINITE" TAB30, "TRACK LENGTH QUARTZ" LIN1;
320 PRINT TAB6,U,TAB30,Q
330 PRINT LIN1 "DISTANCE(MICRONS)" TAB25, "PROBABILITY" TAB50, "ANGLE" TAB60, "N" LIN2;
340 PRINT TAB50,A,TAB60,N
350 REM CHANGE ANGLE TO RADIANS AND DETERMINE ITS SIN AND COS
360 A9=A/10
370 A0=A*PI/180
380 A1=SINA0
390 A2=COSA0
400 I1=INT(10/(DO*A2)-1)
410 REM LOOP TO EVALUATE DISTANCE FROM THE GRAIN BOUNDARY TO THE
420 REM UNIT AREA ON THE POLISHED SURFACE
430 FOR J=1 TO I1
440 DISP J
450 D1=D*A2
460 REM LOOP TO EVALUATE THE PHI INTEGRATION
470 K7=1
480 MAT X=ZER
490 FOR P=(PI/2) TO PI+H2 STEP H2
500 P1=SINP
510 P2=COSP
520 REM LOOP TO SET LIMIT ON RHO INTEGRATION
530 FOR RO=0 TO M1 STEP M1/H2
540 R9=SQR(RO*RO+D1*D1-2*RO*D1*P2)
550 R1=(2*R9*D1*D1)/(R9*R9+D1*D1-RO*RO)
560 R2=R9-R1
570 IF (R1/Q)+(R2/U) >= 1 THEN 610
580 DISP RO
590 NEXT RO
600 REM EVALUATION OF STEP SIZE FOR RHO INTEGRATION
```

```
610 H3=R0/(2*N)
620 REM LOOP TO EVALUATE THE THETA INTEGRATION
630 K6=1
640 MAT Y=ZER
650 FOR T=0 TO (2*PT)+H1 STEP H1
660 T1=SINT
670 T2=COST
680 REM LOOP TO EVALUATE THE RHO INTEGRATION
690 IF R0=0 THEN 950
700 H3=R0/(2*N)
710 K5=1
720 MAT Z=ZER
730 FOR R=0 TO R0+H3 STEP H3
740 F=R^2*P1*(ABS(A1*(D1-R*P2)-R*P1*T2*A2))
750 G=(SQR(D1^2+R^2-2*D1*R*P2))^3
760 Z(K5)=F/G
770 K5=K5+1
780 NEXT R
790 REM EVALUATE SIMPSON'S APPROXIMATION FOR RHO INTEGRATION
800 Y(K6)=FNAN
810 K5=K5+1
820 NEXT T
830 REM EVALUATE SIMPSON'S APPROXIMATION FOR THETA INTEGRATION
840 X(K7)=FNBN
850 K7=K7+1
860 NEXT P
870 REM EVALUATE SIMPSON'S APPROXIMATION FOR PHI INTEGRATION
880 S(J)=FNCN
890 T(J)=0
900 REM PRINT NUMERICAL VALUE OF THE PROBABILITY FUNCTION FOR
910 REM THIS DISTANCE FROM THE GRAIN BOUNDARY AND PROCEED TO NEXT DISTANCE
920 PRINT TAB6,T(J),TAB25,S(J)
930 D=0+00
940 NEXT J
950 REM INPUT WHERE DATA IS TO BE STORED
960 DISP "STOREDATA IN TRACK#, FILE#";
970 INPUT F1,F
980 STORE DATA #F1,F
990 DISP "DO YOU WISH TO INPUT NEW DATA";
1000 INPUT O
1010 IF O=1 THEN 80
1020 END
1030 REM SUBROUTINE TO EVALUATE SIMPSON'S APPROXIMATION FOR RHO INTEGRATION
1040 DEF FNA(N)
1050 L=M=0
1060 FOR K=2 TO 2*N STEP 2
1070 L=Z(K)+L
1080 IF K=2*N THEN 1100
1090 M=Z(K+1)+M
1100 NEXT K
1110 RETURN H3/3*(Z(1)+4*L+2*M+Z(2*N+1))
1120 REM SUBROUTINE TO EVALUATE SIMPSON'S APPROXIMATION FOR THETA INTEGRATION
1130 DEF FNB(N)
1140 L=M=0
1150 FOR K=2 TO 2*N STEP 2
1160 L=Y(K)+L
1170 IF K=2*N THEN 1190
1180 M=Y(K+1)+M
1190 NEXT K
1200 RETURN H2/3*(Y(1)+4*L+2*M+Y(2*N+1))
1210 REM SUBROUTINE TO EVALUATE SIMPSON'S APPROXIMATION FOR PHI INTEGRATION
1220 DEF FNC(N)
1230 L=M=0
1240 FOR K=2 TO 2*N STEP 2
1250 L=X(K)+L
1260 IF K=2*N THEN 1280
1270 M=X(K+1)+M
1280 NEXT K
1290 RETURN H1/3*(X(1)+4*L+2*M+X(2*N+1))
1300 END
```

Once maximum track lengths for the two minerals used and the angle α have been estimated, the total probability (P_f) may be calculated for a specific unit area. By computing P_f for a series of unit areas at varying distances from the grain boundary, curves are generated showing the dependence of P_f on distance (Figure A-5). To find the dependence of track density as a function of distance from the grain boundary, the following equality is used:

$$\rho_S = A \, (N_V C^{238}) \, (\eta^{238})(\lambda_F) \, P_f$$

where

ρ_S = track density per unit area

A = age in years

$N_V C^{238}$ = number of ^{238}U atoms per unit volume

η^{238} = etching efficiency for the detector mineral and crystallographic orientation.

λ^F = decay constant for the spontaneous fission of ^{238}U.

P_f = probability per unit area for a fragment to pass through the unit area at a specified distance from the grain boundary.

This relationship can be rearranged to show the dependence of the age on the track density at a given distance from the grain boundary when values of $N_V C^{238}$ and ^{238} are known. This yields:

$$A = \frac{\rho_S}{P_f} \; \frac{1}{(N_V C^{238})(\eta^{238})(\lambda_F)} \; .$$

However, since obtaining a value for $N_V C^{238}$ is often very difficult, it is best to use a different approach when determining the age of formation for a sample. By using the curves generated to show track density as a function of
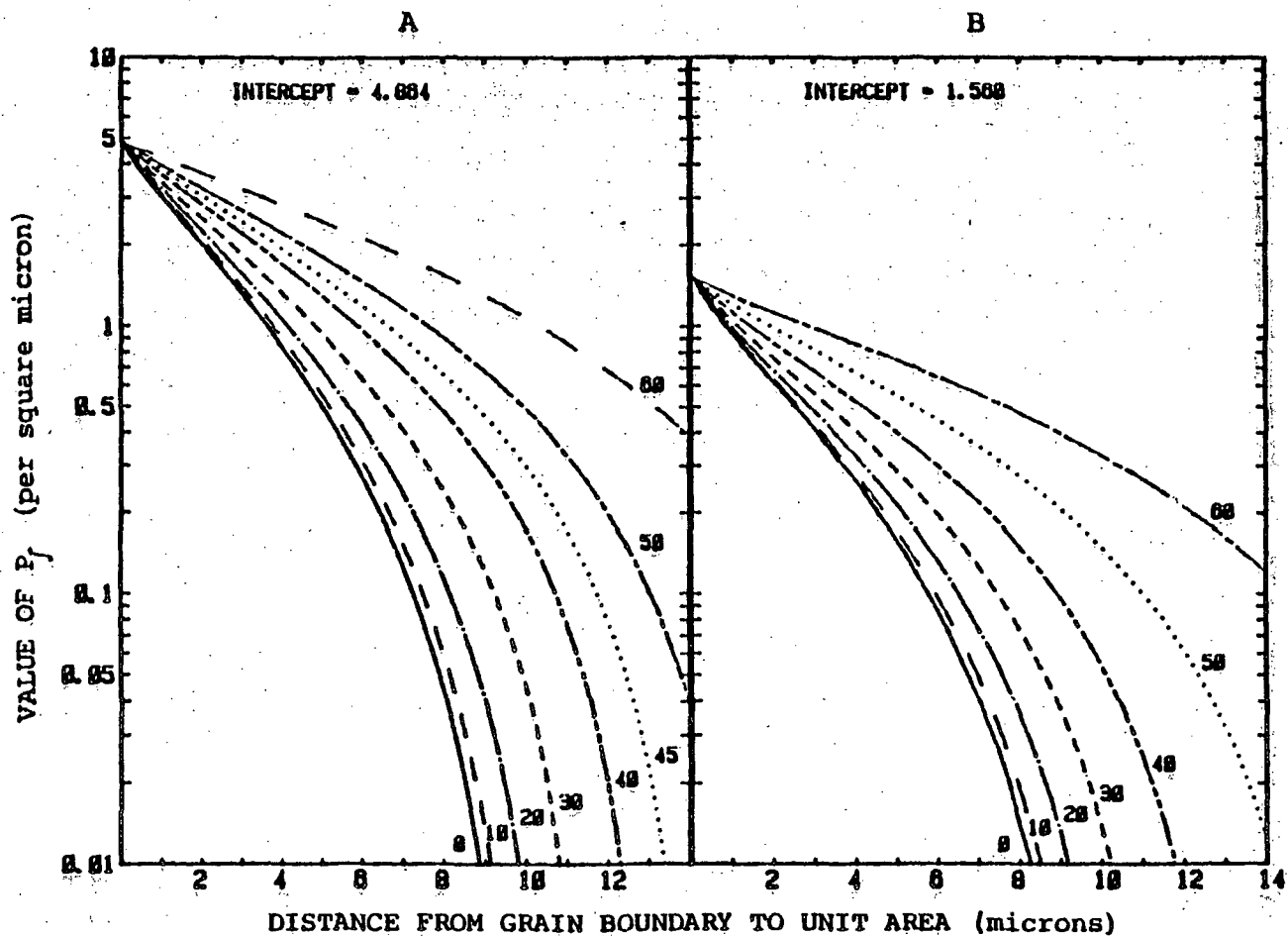
Figure A-5. Theoretical curves determined from the numerical evalua-
tion of the P_f integral for the various grain boundary angles (degrees).
A represents the case where the average fission fragment travel distance
is 10 microns in both the U-rich and U-poor phases, whereas B illustrates
the case where the travel distance is 3 microns in the U-rich phase and
10 microns in the U-poor phase.

distance and then fitting these curves to the data, an intercept value may be determined. The intercept represents the expected track density at the grain boundary. By placing the same sample into a reactor with a mica detector on the polished surface, then inducing the fission of ^{235}U, an induced track density may be counted in the mica detector. This allows the use of the general fission track dating equation

$$A = \frac{1}{\lambda_D} \ln \left[1 + \frac{\rho_s}{\rho_i} \left(\frac{\lambda_D (\phi\, \sigma)\, I}{\lambda_F} \right) \right]$$

where

A = age in years

λ_D = total decay constant for ^{238}U (1.54 x 10^{-10}/yr)

λ_F = decay constant for spontaneous fission of ^{238}U (7.03 x 10^{-17}/yr)

ϕ = neutron dose from irradiation

σ = thermal neutron fission cross section for ^{235}U (582 x $10^{-24}cm^2$)

I = atomic ratio of $^{235}U/^{238}U$ (7.26 x 10^{-3})

(Naeser, 1976)

in determining an age of contact between the two minerals, assuming no track annealing has occurred, avoiding the possible problems with the $N_v C^{238}$ term.

APPENDIX B - Quartz experiments to develop procedures and techniques.

The following describes two experiments performed to evaluate the theoretical model, determine etching characteristics of quartz, and to develop the required procedures and techniques for this fission track dating method. The first experiment uses a slabbed single quartz crystal to determine the etching characteristics for various crystal orientations. The second experiment uses reactor-induced ^{235}U fission, simulating a natural system, to evaluate the theoretical model.

252 Cf IRRADIATED QUARTZ SAMPLES

A ^{252}Cf source was used to induce fission tracks in quartz to better understand its etching characteristics. One experiment was carried out to determine etching efficiencies for various crystallographic orientations, while the other experiment measured track lengths and track diameters as a function of etching time.

Etching Efficiency for Quartz

Etching efficiency (η) is defined as

"the fraction of tracks intersecting a given surface that are etched on the surface under specified conditions" (Fleischer and others, 1975, p. 58).

Since the η^{238} has been established at ~1 for a mica detector (C. W. Naeser oral commun., 1977), the number of tracks etched in the oriented quartz samples were compared to the number of tracks etched in mica detectors irradiated on the same ^{252}Cf source.

Sample Preparation

A large single quartz crystal was slabbed paralled to represented crystal faces (Figure B-1). Several slabs were also cut perpendicular to the C-axis from the remaining crystal core. The slabs were then mounted on glass slide and polished on a vibro-lap unit with tin oxide for 8 hours. This polishing method reduced the problem of crowning found when hand polished on a diamond wheel.

Sample Irradiation

The polished quartz slabs where then placed in direct contact with a ^{252}Cf source (electroplated onto gold foil) for 24 hours. Three mica detectors were placed on the same ^{252}Cf source, again for 24 hours, during the course of this experiment to determine heterogeneity within the source and for calculation of the etching efficiency for quartz.
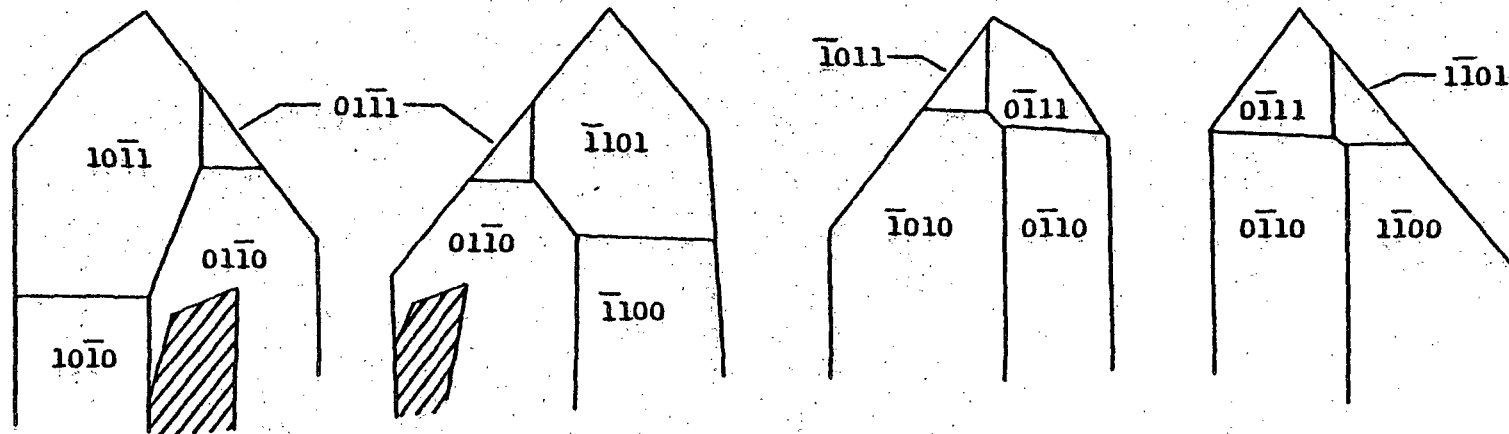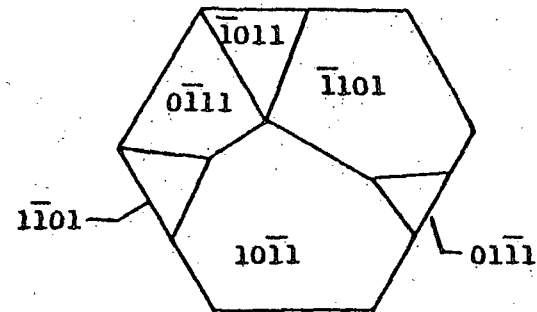
Figure B-1. Diagram indicating indices of crystal faces used in etching characteristic studies. Miller indices determined from descriptions in Dana (1944). To retain natural crystalographic orientations, the crystal was slabbed parallel to these faces.

Sample Etching

The fission tracks in the quartz were then revealed by chemical etching with a 1$\underline{N}$ equimolar solution of NaOH and KOH at 145°C. Etchants previously used for quartz have been described by Fleischer and Price (1964), Sowinski and others, (1972), and Fleischer and others, (1975) with the general conclusion that these etchants are less than satisfactory. Many attempts with HF and $HClO_4$ at several temperatures and concentrations, and various temperatures of NaOH solution were undertaken before the above etchant was decided upon for use in these experiments. The etching apparatus is shown in Figure B-2. The etchant is used until the 145°C temperature can no longer be maintained, suggesting changes in composition and concentration of the solution. The mica detectors were etched in 48% HF for 14 minutes at 25°C.

Track Counts

Each of the quartz samples were etched for several different time periods, counting between each additional etching. Because of the heterogeneity of the ^{252}Cf source, tracks in the mica detector (sample no. CF-8-23-78-MC) were counted with an optical microscope on a grid system to determine the best areas to use in counting the quartz samples. From this, an area of 25 fields of view, where 1 field of view $= 8.4 \times 10^{-4} cm^2$, centered over the distribution of fission tracks, has been used for all subsequent track counts (Figure B-3).

Results

The results for the different crystallographic orientations are found in Table B-1 and Figures B-4 through B-6. It can be seen that etching efficiency varies considerably for the different orientations. The orientation perpendicular to the C-axis is easily recognized in polished thin sections and shows a generally consistent, but low etching efficiency of 0.38 (Figure
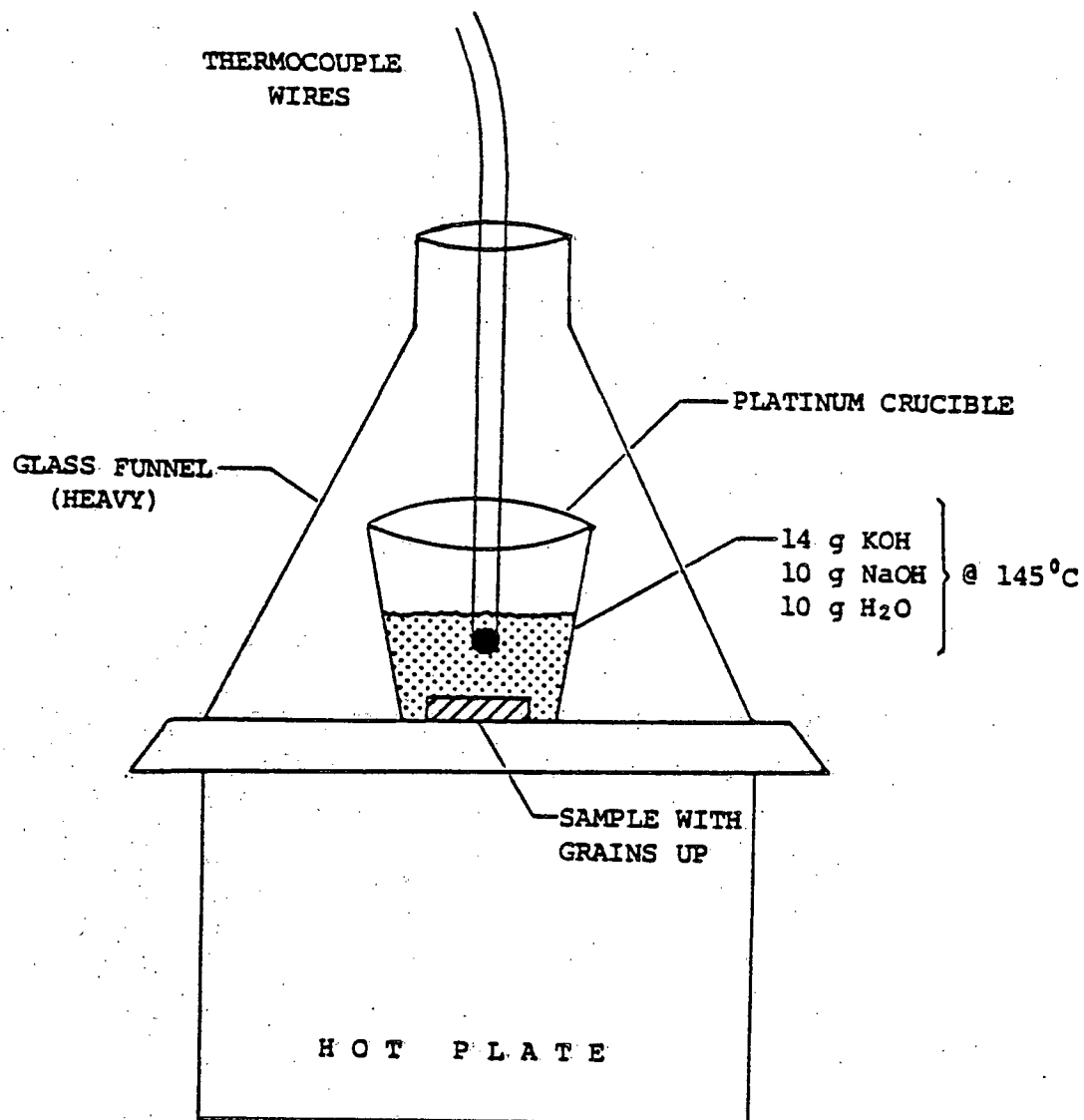
THERMOCOUPLE
WIRES

PLATINUM CRUCIBLE

GLASS FUNNEL
(HEAVY)

14 g KOH
10 g NaOH } @ 145°C
10 g H_2O

SAMPLE WITH
GRAINS UP

HOT PLATE

Figure B-2. Diagram illustrating apparatus used
for etching quartz grains.

AREA CONTAINING INDUCED
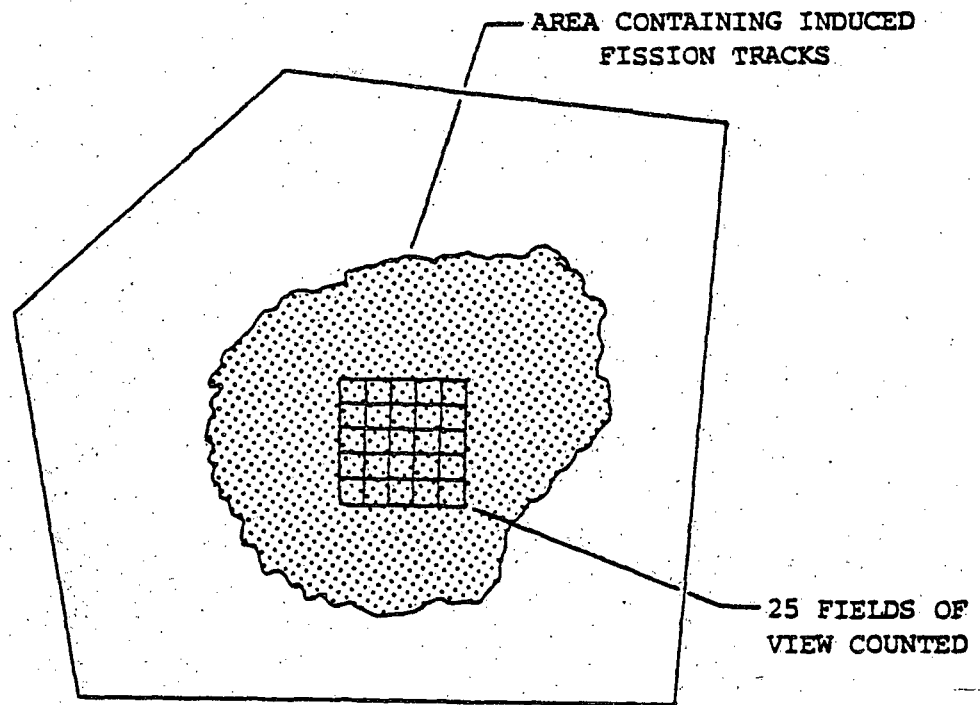FISSION TRACKS

25 FIELDS OF
VIEW COUNTED

Figure B-3. Schematic diagram illustrating area
counted to determine average track density in the
oriented quartz crystals for the experiment on
etching characteristics.

TABLE 8-1

Track density in oriented quartz and mica used for
determination of etching efficiency in quartz.
Tracks counted with optical microscope. Uncertainties
are shown as ±2σ.

Sample Number	Orientation	Etching Time (minutes)	Tracks/cm² (x 10⁶)
MICA			
CF-10-30-78-MS	001	14 (HF)	10.9 ± 2.4
CF-8-23-78-MS	001	14 (HF)	11.4 ± 2.2
CF-6-1-78-MS	001	14 (HF)	10.9 ± 1.6
QUARTZ			
R(#3)a	$10\bar{1}1$	8	3.8 ± 1.8
R(#2)		10	3.4 ± 1.6
R(#1)		15	8.6 ± 1.7
R(#4)a		20	6.8 ± 1.4
R(#5)		30	8.0 ± 1.3
R(#4)b		40	4.2 ± 1.0
R(#3)b		45	2.8 ± 1.0
R'(#3)	$\bar{1}101$	20	10.0 ± 1.7
R'(#5)a		30	10.0 ± 1.1
R'(#5)b		45	3.9 ± 1.3
R"(#1)	$0\bar{1}11$	45	9.4 ± 0.9
Z"(#1)a	$01\bar{1}1$	20	7.9 ± 1.5
Z"(#1)b		30	6.5 ± 1.6
Z"(#1)c		40	8.8 ± 1.3
M₁(#1)a	$\bar{1}010$	15	4.6 ± 1.7
M₁(#4)a		16	2.8 ± 1.1
M₁(#5)a		20	4.2 ± 1.8
M₁(#1)b		25	10.4 ± 1.8
M₁(#5)b		28	7.3 ± 3.4
M₁(#2)a		30	5.0 ± 0.9
M₁(#2)b		38	6.1 ± 1.9
M₁(#4)b		45	3.4 ± 1.1

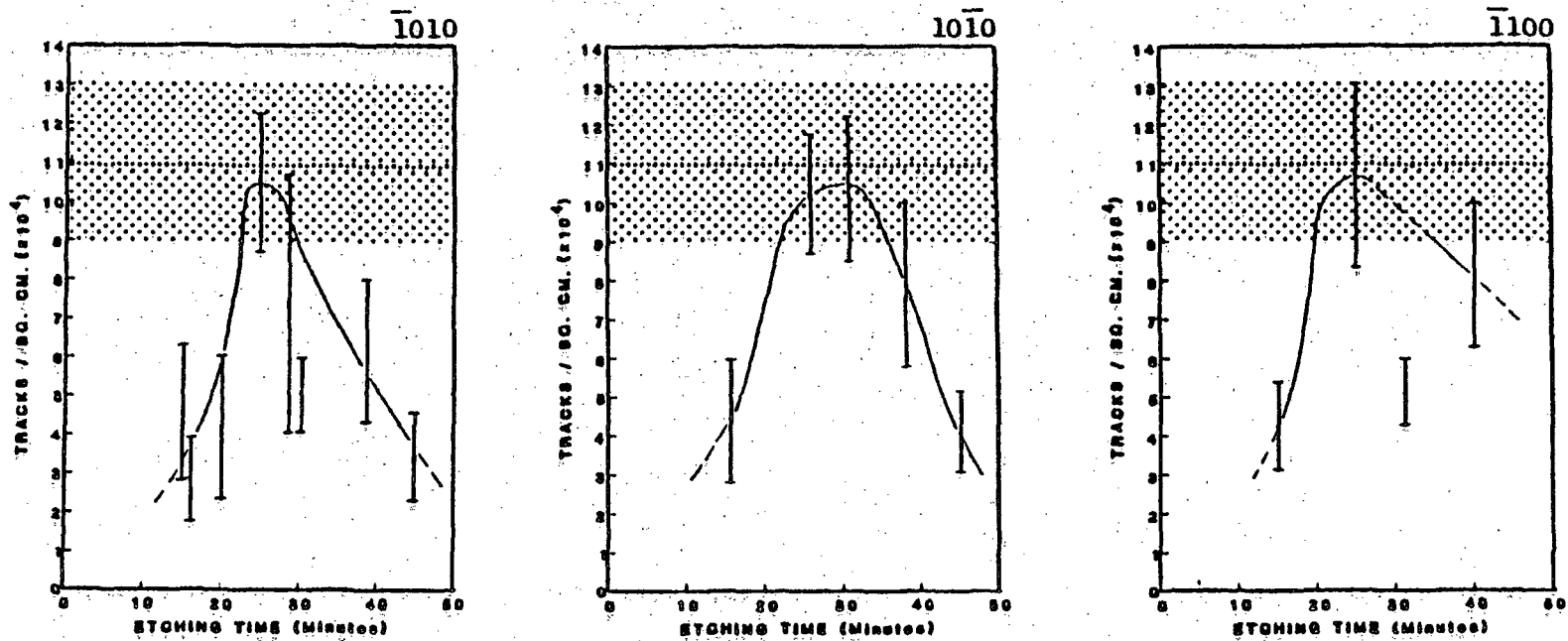| Sample Number	Orientation	Etching Time (minutes)	Tracks/cm² (x 10⁶)
QUARTZ			
M₂(#3)	$1\bar{1}00$	12	3.0 ± 0.6
M₂(#2)a		20	5.1 ± 1.1
M₂(#2)b		30	6.8 ± 2.8
M₂(#1)		40	4.3 ± 1.2
M₃(#3)a	$01\bar{1}0$	20	3.1 ± 0.6
M₃(#1)		30	8.3 ± 3.2
M₃(#3)b		40	5.1 ± 1.0
M₁'(#1)a	$10\bar{1}0$	15	4.6 ± 1.7
M₁'(#1)b		25	10.4 ± 1.8
M₁'(#2)a		30	10.6 ± 2.0
M₁'(#1)c		38	7.9 ± 2.2
M₁'(#2)b		45	4.0 ± 1.0
M₂'(#1)a	$\bar{1}100$	15	4.3 ± 1.1
M₂'(#1)b		22	10.7 ± 2.4
M₂'(#2)a		30	5.1 ± 0.9
M₂'(#2)b		40	8.1 ± 1.9
$\bar{1}$C(#3)a	$000\bar{1}$	16	3.0 ± 0.9
$\bar{1}$C(#4)a		20	2.7 ± 0.6
$\bar{1}$C(#3)b		25	4.2 ± 0.7
$\bar{1}$C(#2)		30	4.1 ± 0.6
$\bar{1}$C(#4)b		38	3.9 ± 0.8
$\bar{1}$C(#1)		45	3.2 ± 1.0

Figure B-4. Plots of track density versus etching time for data from the ^{252}Cf irradiated quartz samples to determine etching efficiency of quartz relative to mica standards for indicated crystal faces. The stippled bands represent the track density found in mica standards ($11 \pm 2 \times 10^4$ tracks/ cm^2).
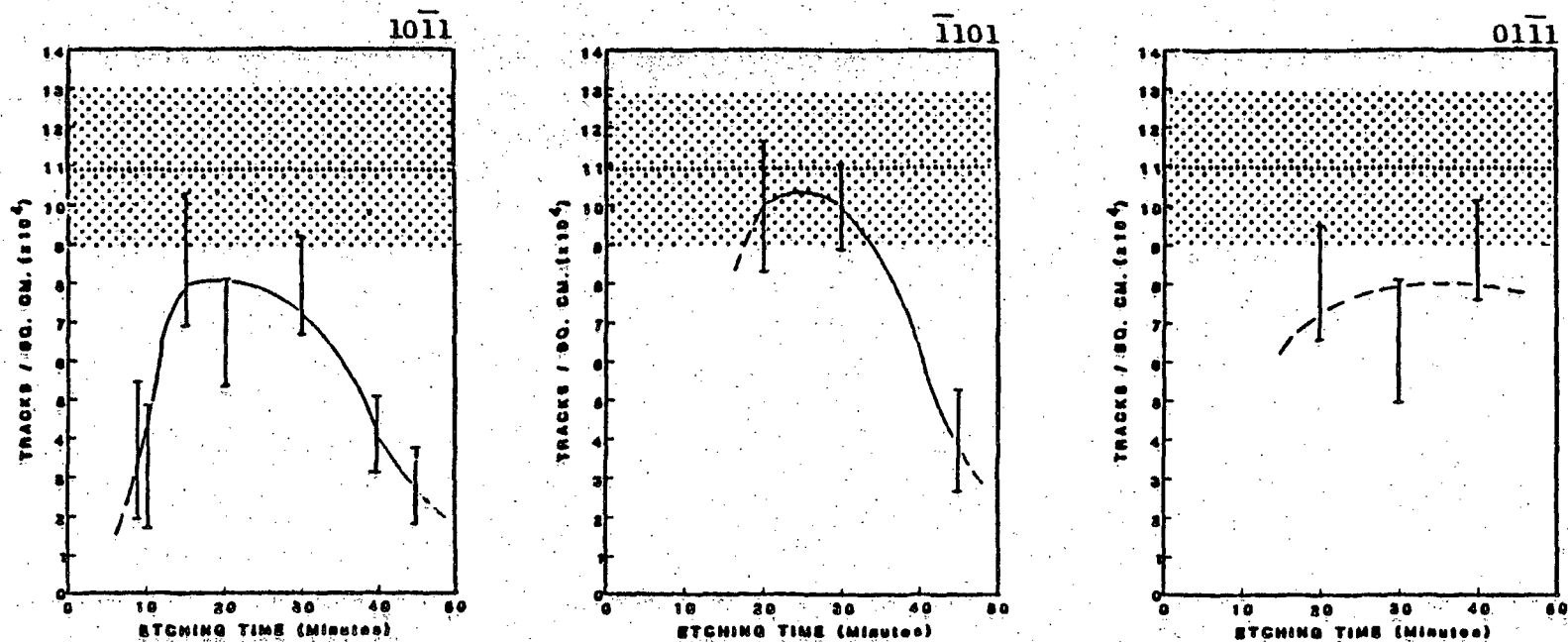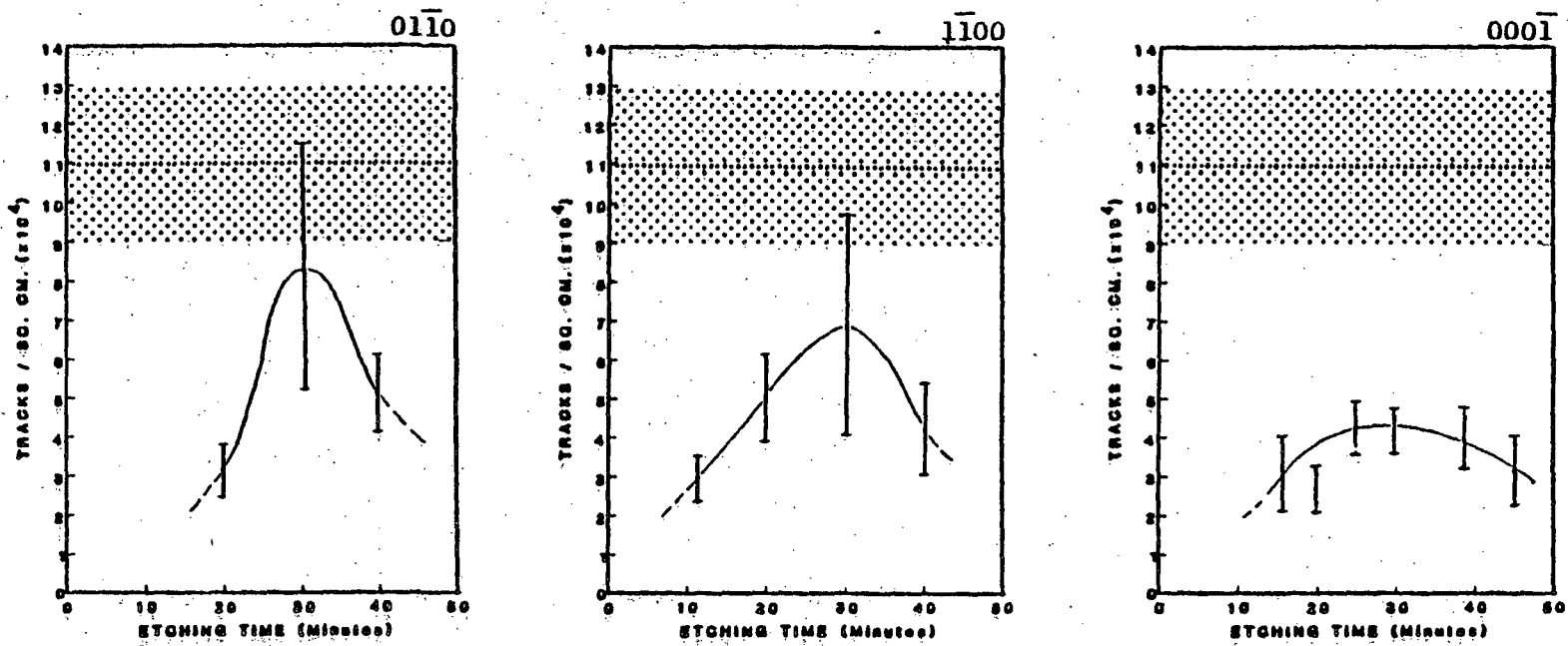
Figure B-5. Plots of track density versus etching time for data from the ^{252}Cf irradiated quartz samples to determine etching efficiency of quartz relative to mica standards for indicated crystal faces. The stippled bands represent the track density found in mica standards ($11 \pm 2 \times 10^4$ tracks/cm^2).

Figure B-6. Plots of track density versus etching time for data from the ^{252}Cf irradiated quartz samples to determine etching efficiency of quartz relative to mica standards for indicated crystal faces. The stippled bands represent the track density found in mica standards ($11 \pm 2 \times 10^4$ tracks/ cm^2).

B-6). This etching efficiency may not be valid for the shorter etching times used for very high track densities and TEM observation. However, results from the Midnite Mine sample (see text) indicate that this value for n^{238} is justified.

TRACK LENGTH AND DIAMETER

Employing the quartz samples from the previous experiment, replicas were made of the etched surface at the various etching times and prepared for observation in the SEM as follows.

Sample Preparation

Replication of the etched surface was accomplished using cellulose acetate softened with a drop of acetone placed on the sample surface (Figure B-7). When the acetone had completely evaporated (~20 minutes), the plastic replica was carefully peeled off and taped to a SEM conductive stub. The replica and stub were then coated in an evaporative system with 200-400 Å of Au-Pd or Au to produce a conductive surface. This replication procedure produces a negative image of the etched surface, allowing the entire track length and diameter to be observed.

Results

Track diameter and track length as a function of etching time were then determined for several crystal orientations (Table B-2). From Figure B-8, it can be seen that track lengths show a dramatic increase at etching times between 20 and 30 minutes, whereas track diameters increase linearly to about 40 minutes where bulk sample attack begins enlarging track diameters at a greater rate than the track lengths. This suggests that, for optical observation, optimal etching time is 20 to 30 minutes. This was also seen in the etching efficiency curves (Figures B-4 and B-6) where a maximum track density generally occurs within this 20 to 30 minute etching period.
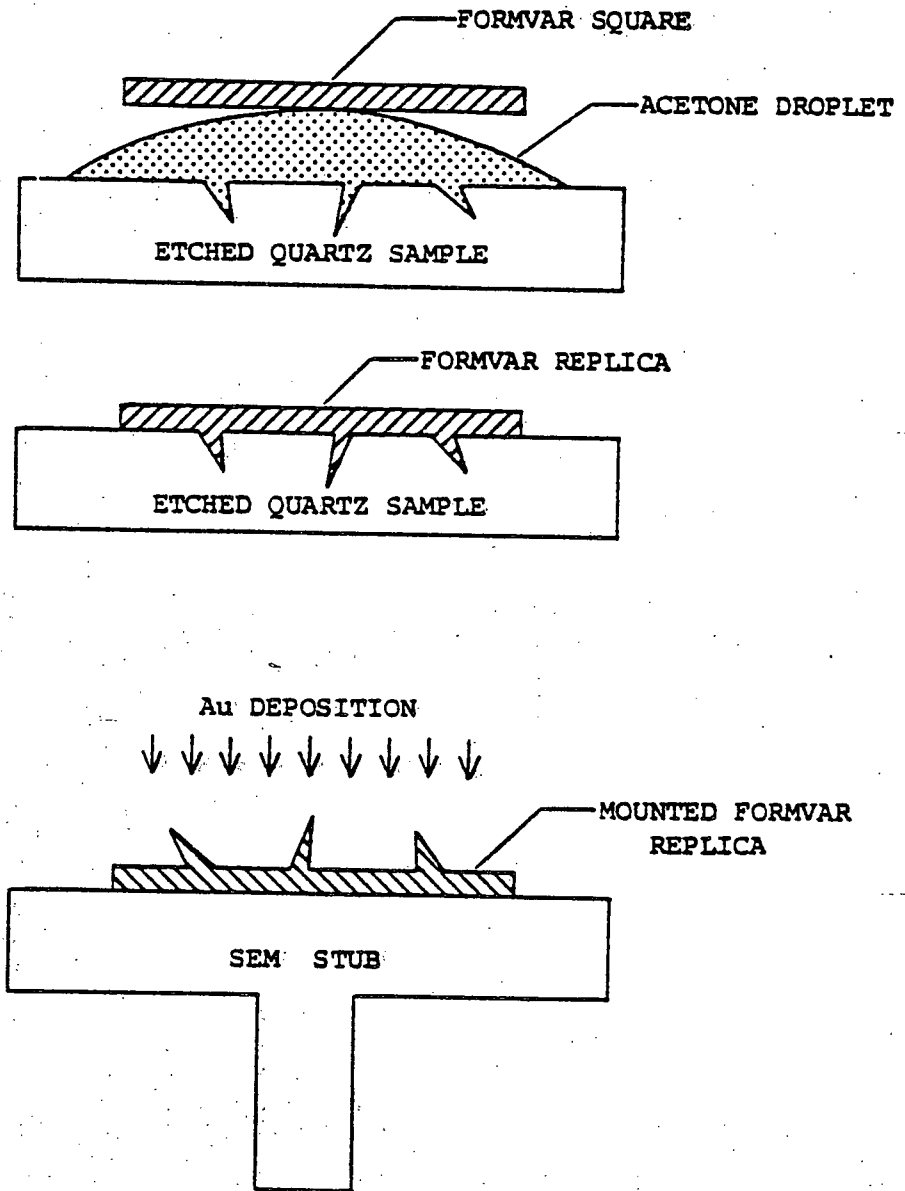
FORMVAR SQUARE

ACETONE DROPLET

ETCHED QUARTZ SAMPLE

FORMVAR REPLICA

ETCHED QUARTZ SAMPLE

Au DEPOSITION

MOUNTED FORMVAR
REPLICA

SEM STUB

Figure B-7. Replication of etched sample surface
using acetone-softened Formvar (cellulose acetate),
and subsequent mounting and coating for observa-
tion in SEM.

TABLE B-2

Fission track etching rates in quartz. Measured using plastic replicas of the tracks and observation with a scanning electron microscope. Uncertainties are shown as ±2σ.

| Crystal Orientation	Etching Time (minutes)	Track Diameter (microns)	Track Length (microns)
$\bar{1}$010, 1$\bar{1}$00, 01$\bar{1}$0	8	0.15 ± 0.10	
	10	0.20 ± 0.20	
	12	0.15 ± 0.10	
	15	0.28 ± 0.10	0.96 ± 0.20
	16	0.30 ± 0.10	0.95 ± 0.10
	20	0.55 ± 0.20	
	25	0.70 ± 0.20	3.20 ± 0.80
	45	1.60 ± 0.30	7.20 ± 1.00
10$\bar{1}$0, $\bar{1}$100	8	0.10 ± 0.10	0.30 ± 0.10
	15	0.27 ± 0.10	0.80 ± 0.10
	20	0.60 ± 0.20	
	40	1.00 ± 0.30	
	45	1.50 ± 0.20	6.50 ± 1.00
10$\bar{1}$1, $\bar{1}$101	8	0.15 ± 0.10	0.35 ± 0.10
	10	0.25 ± 0.10	0.70 ± 0.20
	15	0.29 ± 0.10	0.85 ± 0.20
	20	0.50 ± 0.20	1.45 ± 0.30
	30	0.75 ± 0.20	5.40 ± 0.80
	45	0.90 ± 0.30	7.00 ± 1.00
000$\bar{1}$	4	0.03 ± 0.01	0.15 ± 0.05
	8	0.15 ± 0.10	0.39 ± 0.10
	16	0.25 ± 0.10	0.80 ± 0.20
	20	0.39 ± 0.10	1.40 ± 0.30
	30	0.80 ± 0.20	5.60 ± 0.80
	45	1.80 ± 0.50	6.80 ± 1.00
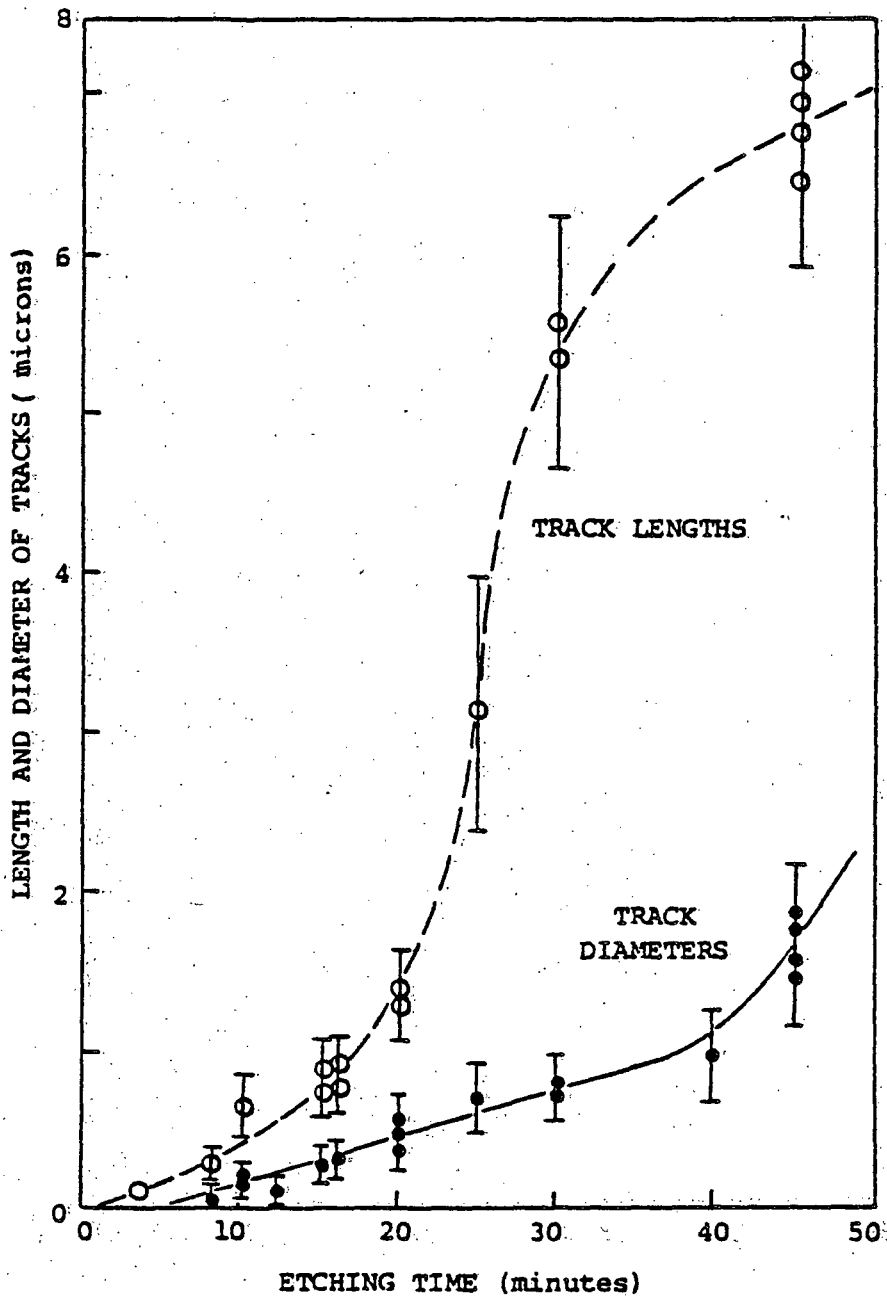
Figure B-8. A plot illustrating etching time versus track length and track diameter from quartz etching studies.

REACTOR-IRRADIATED QUARTZ SAMPLES

To develop the procedures and techniques required for dating natural samples, and to check the validity of the theoretical model, quartz grains in a uranium solution of known U-concentration (natural isotopic composition) were irradiated with thermal neutrons in a reactor to induce ^{235}U fission. This experiment allowed close approximation of a natural system, with the major differences being induced ^{235}U fission instead of the spontaneous fission of ^{238}U and a U-solution instead of uraninite for the U-rich phase.

Sample Preparation and Irradiation

Quartz crystals were crushed to 80-120 mesh, then hand picked for uniformity of spherical shape. Thirty to fifty of these selected grains were weighed into a polyethylene vial with a weighed HNO_3 solution of 1.202 mg natural uranium per gram of solution. The vials were then placed into reactor tubes, cushioned with tissue paper, and irradiated in the "Lazy Susan" reactor at the Denver Federal Center. The samples received a neutron dose of 9.46 x 10^{16} neutrons/cm^2, which corresponds to a grain boundary track density of 1.97 $\pm$ 2 x 10^9 tracks/cm^2 using the empirical formula:

$$\rho_T = \frac{U \ (\phi)}{5.76 \ x \ 10^{10}}$$

where

ρ_T = track density at grain boundary

U = uranium concentration in ppm

ϕ = neutron dose in neutrons/cm^2*

When the samples had cooled to near-background levels of radiation, the U-solution was drained and discarded and the quartz grains thoroughly rinsed with water and ethanol.

*believed to have an uncertainty of $\pm$10 percent

Mounting, Polishing and Etching Grain Mounts

The grains were then mounted using the method described by Naeser (1976):
5-15 grains were placed on a teflon sheet, and several drops of epoxy added to
the grains a glass slide marked with sample numbers was placed on top, using
spacers to level the glass slide (Figure B-9), and the epoxy was allowed to
harden. The grain mounts were polished using the procedure described by
Naeser (1976): Coarse emery paper was used to expose an interior surface of
the quartz grains; and the samples were then unidirectionally polished,
alternating 90° with each decreasing abrasive to the final abrasive of one
micron diamond paste. This polishing procedure allows scratch marks to be
distinguished from fission tracks.

The fission tracks were revealed by the chemical etching procedure
described in the previous section.

Observation and Counting of Tracks

Observation and counting of tracks was accomplished using a scanning
electron microscope (SEM) after the samples had been mounted on a conductive
SEM stub and coated as described in the previous section. Due to inherent
problems with the SEM's operation, the inability to "see into" the etched
track is a major disadvantage of using this machine. Discrimination between
crystal defects, polish scratches, and fission tracks may therefore be
difficult, if not impossible. Resolution of the SEM also limits its use to
track densities generally less than 10^{6} tracks/cm^2.

Replication of etched surface as described in the previous section
eliminates most of these problems, but heat from the electron beam tends to
destroy the replica causing a problem with obtaining accurate track
densities. Therefore, for natural samples where track densities are expected
to be greater than 10^{9} tracks/cm^2, procedures for the transmission
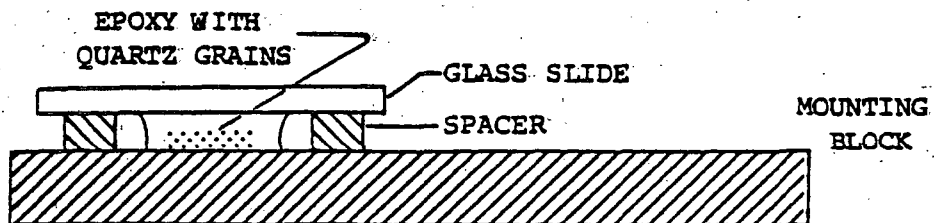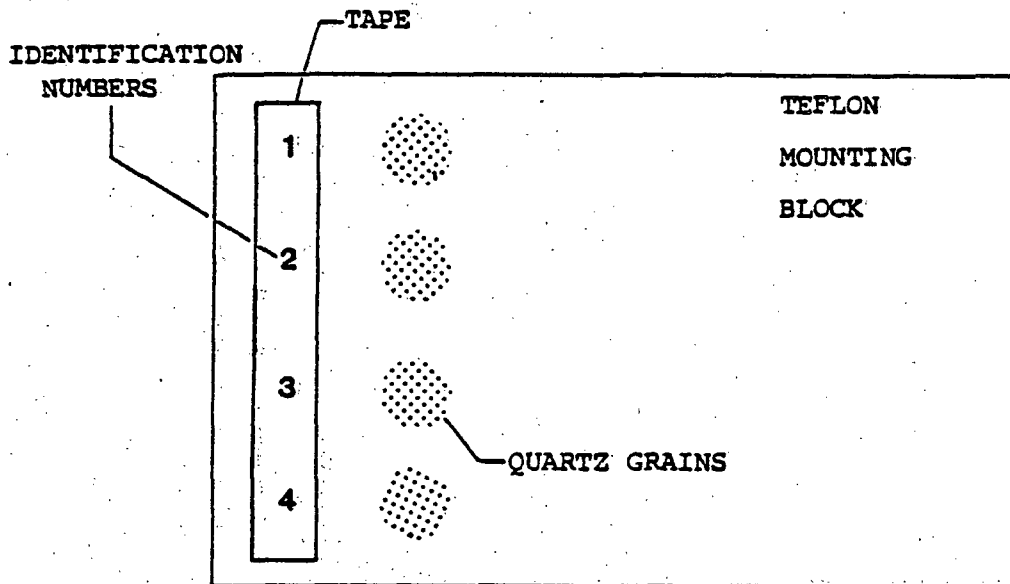
Figure B-9. Diagram illustrating mounting procedure
for quartz grains with epoxy (After Naeser, 1975).

electron microscope (TEM) were also developed using these irradiated quartz samples.

TEM Specimen Preparation

Since the electron beam must pass through the specimen viewed, the TEM requires a two stage replicating procedure to observe the fission tracks. To make a two stage replica, first the sample is replicated with cellulose acetate as previously described for the SEM, then this plastic replica is taped, replicated side upwards, to a glass slide. This is placed into an evaporative coating system. First, 20-50 $\overset{o}{A}$ of metal (Pd or Pf) is shadow coated at an angle of 20-30° from the horizontal (Figure B-10). The formula for calculation of evaporaive coating thickness is:

$$t = \frac{m \ (3 \ \sin \ \epsilon) \ (10^8)}{16 \ \pi \ r^2 \ d}$$

where

m = mass of material (g)

t = thickness of deposit (A)
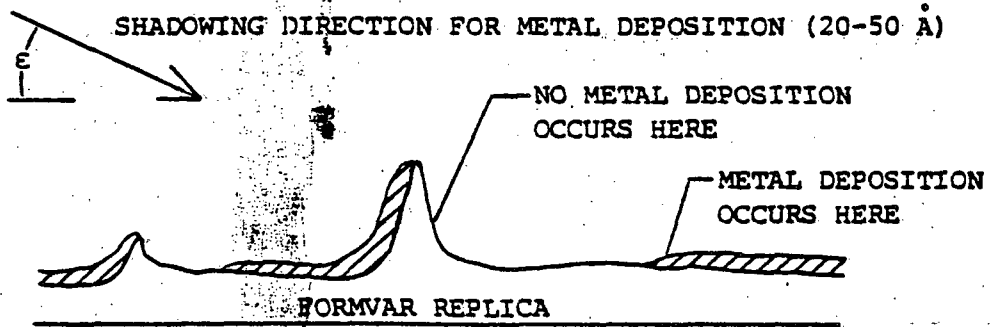
ϵ = shadowing angle (radians)

r = distance from source to specimen (cm)

d = density of material (g/cm^2)

(Kay, 1965)

This coating increases the contrast of the final TEM specimen. Next, a 200-400 $\overset{o}{A}$ carbon coating is evaporated uniformly onto the sample surface. The plastic replica is then dissolved leaving only the metal-carbon replica. The plastic replica is dissolved using methyl acetate by transferring the replica through four such solutions to remove all the plastic residue from the metal-carbon replica. This replica must then be "fished" onto a 100 or 200 mesh copper TEM grid and dried.

S T E P 1

SHADOWING DIRECTION FOR METAL DEPOSITION (20-50 Å)

ε

NO METAL DEPOSITION
OCCURS HERE

METAL DEPOSITION
OCCURS HERE

FORMVAR REPLICA

S T E P 2

1 0 0 - 2 0 0 Å C A R B O N

CARBON COATING
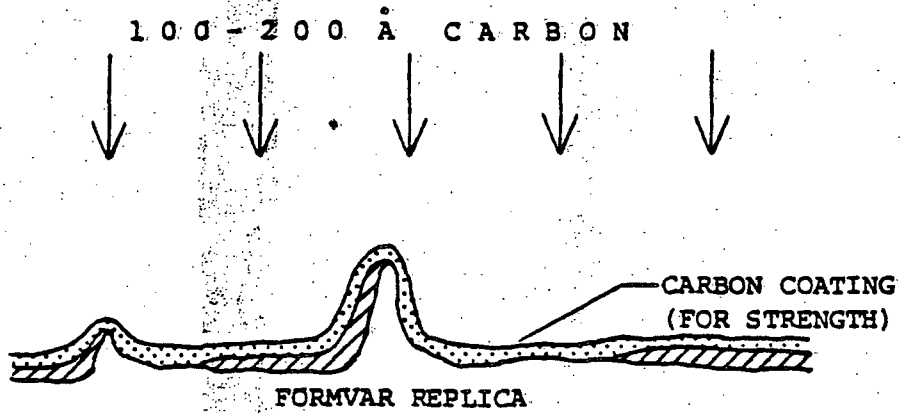(FOR STRENGTH)

FORMVAR REPLICA

Figure B-10. Diagramatic representation of shadowing
two stage replica to improve contrast for TEM observa-
tion.

TEM Observation and Counting

Photomicrographs of the grains show the etched tracks as light-colored spikes. It can be seen also from the photomicrographs that indicate track densities do indeed decrease with distance from the grain boundary. Track densities computed from the photomosaics at several distances from the grain boundary are shown in Table B-3. Since fission events follow a Poisson distribution (Naeser, 1976), where the standard deviation is the square root of the number of tracks counted, the track density counts were pooled, where possible, to improve the statistics.

Results

Results from these experimental quartz grains are plotted in Figures B-11 and B-12. The intercepts of 18.4, 18.5, and 19.3 tracks/μm^2 show excellent agreement with the calculated track density of 19.7 $\pm$ 2 tracks/μm^2 from the reactor irradiation. Data shown in Figures B-12 from sample #9-12-4FC show no correlation with any of the theoretical curves, and the sharp drop in track density at a distance of 6 microns indicates that this sample may have had another quartz grain in very close proximity when irradiated, yielding the misleading results.

Another noteworthy observation concerns the decrease in track density for distances of less than 2 microns from the grain boundary. This is due to the increased relative etching rate at the corner of a crystal, which is being etched from two surfaces instead of one. This increased bulk etching rate is nearly equal to or greater than the track etching rate, causing the reduction in size and number of tracks at the grain boundary. Therefore, for dating natural samples, track densities were only used for distances greater than 2 microns from the grain boundary to minimize this effect.

TABLE B-3

Results from traverses on reactor irradiated quartz grains.
Calculated track density at the grain boundary equals 19.7
tracks/μm^2 from irradiation. Track densities are computed
from pooled counts. Uncertainties are shown as $\pm 2\sigma$.

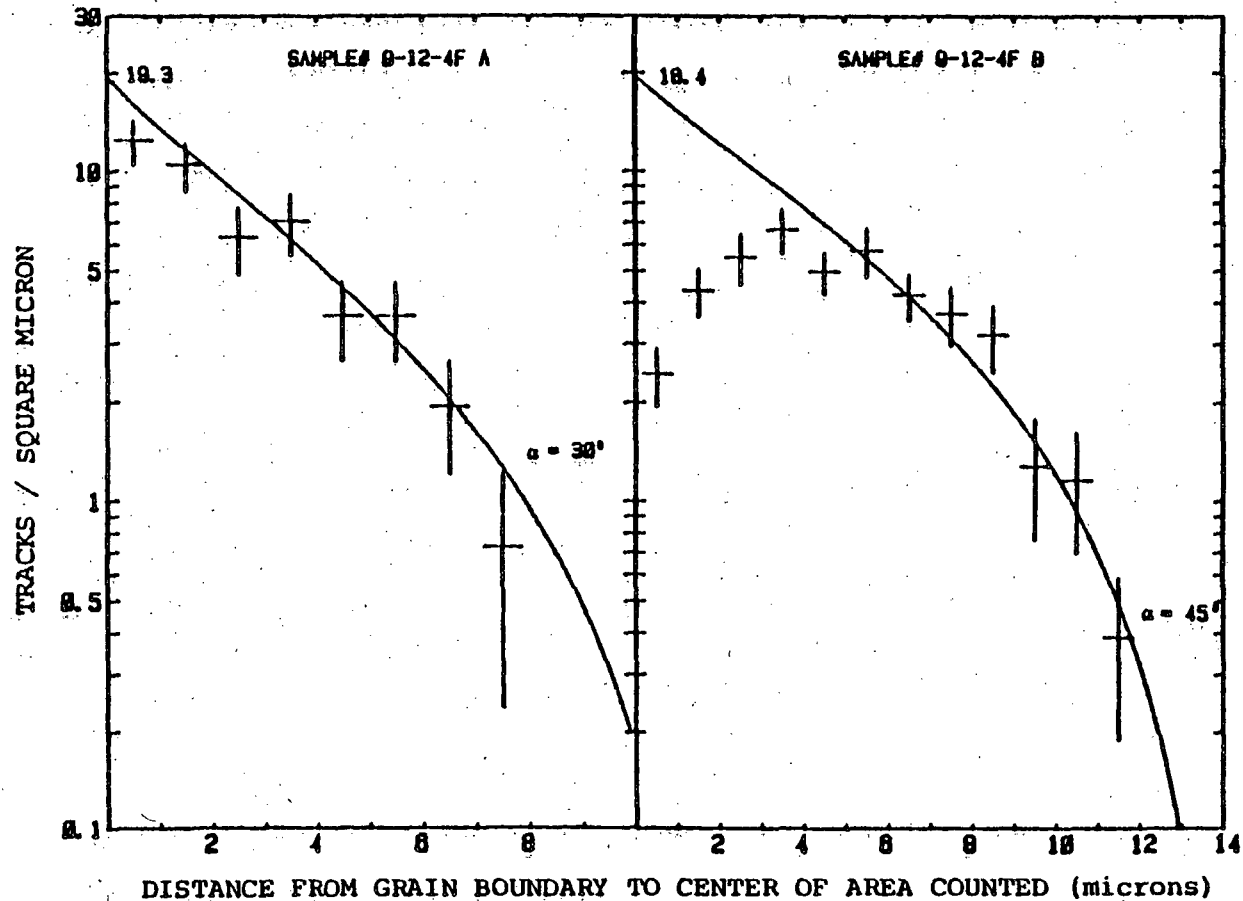| Sample Number	Distance from Grain Boundary to Center of Area Counted (microns)	Track Density (tracks/μm^2)	Calculated Track Density at Grain Boundary (tracks/μm^2)
9-12-4E (A&B)	0.5	6.13 ± 1.40	
	1.5	7.38 ± 1.45	
	2.5	7.25 ± 1.45	
	3.5	4.00 ± 1.25	
	4.5	2.25 ± 0.99	
	5.5	1.56 ± 0.88	
	6.5	0.63 ± 0.58	
	7.5	0.50 ± 0.58	
			18.4
9-12-4F (A)	0.5	12.44 ± 1.95	
	1.5	10.49 ± 1.71	
	2.5	6.34 ± 1.46	
	3.5	7.07 ± 1.46	
	4.5	3.66 ± 0.98	
	5.5	3.66 ± 0.98	
	6.5	1.95 ± 0.73	
	7.5	0.73 ± 0.49	
			19.3
9-12-4F (B)	0.5	2.44 ± 0.49	
	1.5	4.36 ± 0.73	
	2.5	5.52 ± 0.96	
	3.5	6.68 ± 0.99	
	4.5	5.01 ± 0.72	
	5.5	5.78 ± 0.96	
	6.5	4.24 ± 0.67	
	7.5	3.72 ± 0.74	
	8.5	3.21 ± 0.74	
	9.5	1.28 ± 0.51	
	10.5	1.16 ± 0.46	
	11.5	0.39 ± 0.20	
			18.4
9-12-4F (C)	0.5	5.66 ± 1.89	
	1.0	5.66 ± 1.89	
	1.5	6.29 ± 1.99	
	2.0	5.66 ± 1.89	
	2.5	4.40 ± 1.66	
	3.0	3.77 ± 1.54	
	3.5	2.20 ± 1.09	
	4.0	1.26 ± 0.89	
	4.5	1.57 ± 0.99	
	5.0	0.63 ± 0.63	
	5.5	0.31 ± 0.44	
	6.0	0.31 ± 0.44	no correlation with theoretical curves (see explanation in text)

Figure B-11. Plots of track density versus distance from the grain boundary for data from the reactor irradiated quartz samples to test the theoretical model.
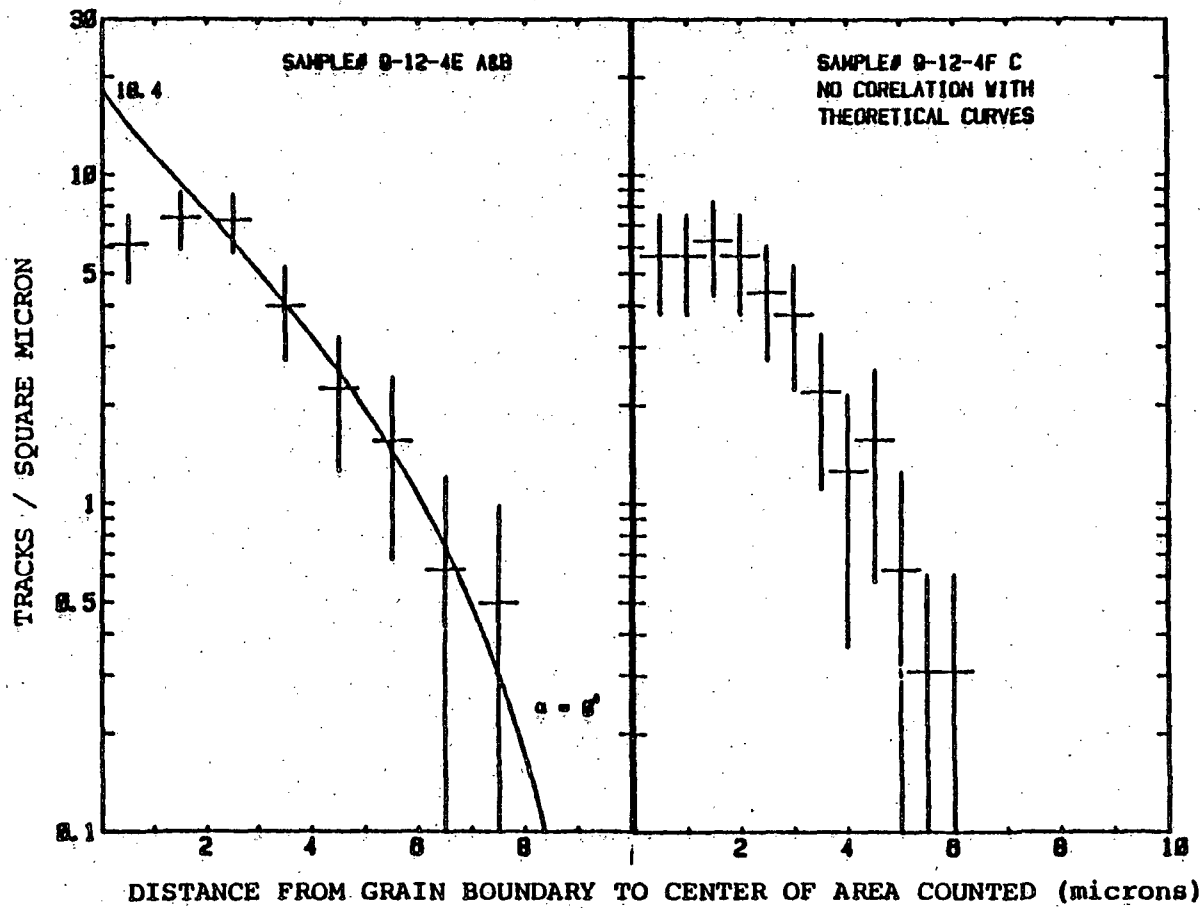
SAMPLE# 9-12-4E A&B

18.4

$\alpha = 0^\circ$

SAMPLE# 9-12-4F C
NO CORELATION WITH
THEORETICAL CURVES

TRACKS / SQUARE MICRON

DISTANCE FROM GRAIN BOUNDARY TO CENTER OF AREA COUNTED (microns)

Figure B-12. Plots of track density versus distance from the grain boundary for data from the reactor irradiated quartz samples to test the theoretical model.

UNITED STATES DEPARTMENT OF THE INTERIOR

GEOLOGICAL SURVEY

Fission Track Dating applied to Uranium Mineralization

Erick F. Weiland, Kenneth R. Ludwig,

Charles W. Naeser, and E. Craig Simmons

Denver, Colorado 80225

Open-File Report 80-380

1980

This report is preliminary, and has not been edited or reviewed for conformity with U.S. Geological Survey standards or nomenclature.

ABSTRACT

The occurrence of quartz adjacent to uraninite in many uranium deposits allows quartz to be employed as a detector to record the spontaneous fission decay of ^{238}U occurring within the adjacent uraninite. A theoretical equation which models the decrease in track density within the quartz with increased distance from the grain boundary with the adjacent uraninite is described in detail. To test this model, quartz grains were placed in a U-solution, irradiated in a reactor to induce ^{235}U fission, and then the track distribution within the quartz determined. The theoretical curves very closely match these data and yield track densities in excellent agreement with the reactor-calculated track density.

Etching experiments on quartz were undertaken to establish values for etching efficiency and etching rates for various crystallographic orientations. Etching efficiency for a plane perpendicular to the c-axis, using KOH-NaOH etching solution at $145^\circ C$, has been determined to be 0.38.

To test this model on natural material, samples from the Midnite Mine, Washington were prepared and dated using quartz associated with uraninite; ages of 52 to 54 m.y were obtained. These ages are in excellent agreement with a previously established U-Pb isochron age of 51.0 ± 0.5 m.y.

INTRODUCTION

To better understand the origin and history of uranium deposits, accurate ages of mineralization are essential. Radiometric age determinations on uranium ores have previously used the U-Pb isotopes (Faure, 1977) and U-series methods (Hamilton and Farquhar, 1968). Discordant results for uranium deposits are commonly obtained by these methods (see Hamilton and Farquhar (1968), Faure (1977), Ludwig (1977), Ludwig and Young (1975) and, Ludwig and others 1977)) because of variance of the mineral system with respect to two basic limiting factors: 1) the closure of the system to loss and gain of the parent and all daughter elements, and 2) lack of sufficiently precise knowledge of the isotopic composition of the initial Pb. Thus a method for determining the age of uranium mineralization involving fewer constraints would be of great value.

The fission-track method of age determination is based upon the fission of ^{238}U atoms into two heavy, highly charged, high velocity fragments. Their passage through most solids creates narrow paths of intense crystal damage on an atomic scale (Fleischer and others, 1975). These damage zones are normally stable in insulating solids over geologic time at low temperatures ($<100^{o}C$) (Naeser, 1976), and may be revealed by use of several techniques, depending on the nature of the solid. A fission-track age is related only to the concentration of ^{238}U, closure of the system to uranium migration, and the stability of tracks. It does not depend upon knowledge of isotopic composition of initial-Pb, or absence of loss or gain of radiogenic-Pb or intermediate decay products. Therefore, fission-track data should yield reliable ages of mineralization for uranium deposits which have been closed to loss or gain of uranium and have remained at temperatures below $100^{o}C$ (to avoid annealing of tracks) since formation.

3

to reach the unit area (see detailed discussion in Appendix A). The total probability is given by the integral

$$P_f = \frac{1}{2\pi} \int_{\pi/2}^{\pi} \int_{0}^{2\pi} \int_{0}^{\rho_\ell} \frac{\left| -\rho \sin\phi \cos\theta \cos\alpha + a \cos\alpha \sin\alpha - \rho \cos\alpha \right| \rho^2 \sin\phi \, d\rho \, d\theta \, d\phi}{(a^2 \cos^2\alpha - 2 a \rho \cos\alpha \cos\phi + \rho^2)^{3/2}} \quad (1)$$

Variables are defined in Appendix A and Figure A-1. This integral must be numerically evaluated due to the absolute value within the numerator, and the dependence of the upper limit for the integration upon the maximum track lengths in the minerals under study. A flow chart, computer program, and generated curves for the numerical evaluation can be found in Appendix A. By plotting track density versus distance from the grain boundary for data from traverses in the detector mineral, and then fitting the theoretical curves to these data, the track density at the grain boundary may be determined. An age (A) may be calculated from this using

$$A = \frac{\rho_s}{(N_v C^{238}) \, \lambda_F \, R^{238} \, \eta^{238}} \quad (2)$$

where

ρ_s = spontaneous fission track density in the interior of the U-rich phase.

$N_v C^{238}$ = number of ^{238}U atoms per unit volume (assumed to be uniformly distributed).

λ_F = decay constant for the spontaneous fission of ^{238}U.

R^{238} = range (average travel distance) of fission fragments in the U-rich phase.

contain the requisite uraninite-quartz relationships. Polished thin sections of the vein samples were prepared and studied to locate the quartz grains to be used for age determinations. Since viewing down the c-axis is an easily recognized orientation in quartz crystals and this orientation produces consistent etching characteristics (Appendix B), grains with this orientation were chosen for study. The other considerations in choosing the specific grain to be used were, first, that little or no uraninite/coffinite intermixing adjacent to the quartz should be indicated by reflected light microscopy, and second that the quartz grain be no less than 50 μm in diameter.

A mica detector was then taped to the polished surface over the entire sample. This package was placed into a reactor tube and irradiated in the U.S Geological Survey "Lazy Susan" position of the TRIGA research reactor in Denver. The sample received a thermal neutron dose of 9.45×10^{11} neutrons/cm^2. The mica detector was then removed from the sample, etched in HF at $25^\circ C$ for 14 minutes, and the induced track density counted so that equation 3 could be used for age calculations.

The Midnite Mine sample was etched in a solution containing 14 g. KOH, 10 g. NaOH, and 10 g H_2O at $145^\circ C$ for 3.5 minutes to reveal the fission tracks (described in detail in Appendix B). Since track densities of 10^9 tracks/cm^2 or greater were expected, counting of tracks required a transmission electron microscope (TEM). A two stage replication technique, modified from Kay (1965), was used in preparation of TEM specimens. Briefly, this technique involves replicating the etched surface with cellulose acetate softened with acetone. When the acetone has evaporated and the cellulose acetate re-hardened, the plastic replica is carefully peeled off the surface. It is generally necessary to do this several times before a satisfactory replica is obtained. The replica is then shadow-coated with a 20-50 $\overset{o}{A}$ metal

Data from the Midnite Mine sample yield the following results. Sample MD-256-EW-3 (A) has an intercept value of 35.2 tracks/μm^2, based on parallel count traverses (Table 1 and Figure 1). Data from sample MD-256-EW-3 (C), based on 6 parallel count traverses within the same quartz grain as MD-256-EW-3 (A), yields an intercept of 36.3 tracks/μm^2 (Table 1 and Figure 2). Sample MD-256-EW-3 (D), yields an intercept of 35.9 tracks/μm^2 based on 1 traverse only (Table 1 and Figure 3). This sample is from another grain which has coffinite/uraninite intermixing problems, as indicated by subsequent ore-microscope examination, and therefore is not included in the final age calculation. Data from sample #MD-256-EW-3 (B) have not been included here because fission tracks were recorded as far as 35 μm into the quartz grain, suggesting an irregular distribution of uraninite surrounding the quartz and an irregular shape of the quartz grain.

Uncertainties for all counts are based on a Poisson distribution for fission events. The relative standard derivation has been determined by taking the square root of the total number of tracks counted and dividing by the total number of tracks counted. All uncertainties given are $\pm$ 2 standard deviations (2σ).

From the reactor irradiation, the induced track density in the mica detector was calculated to be 1.003 x 10^7 tracks/cm^2 using

$$\rho_T = \frac{U \phi}{5.76 \times 10^{10}}$$

where

ρ_T = track density at grain boundary

U = uranium concentration in ppm

ϕ = neutron dose in neutrons/cm^2

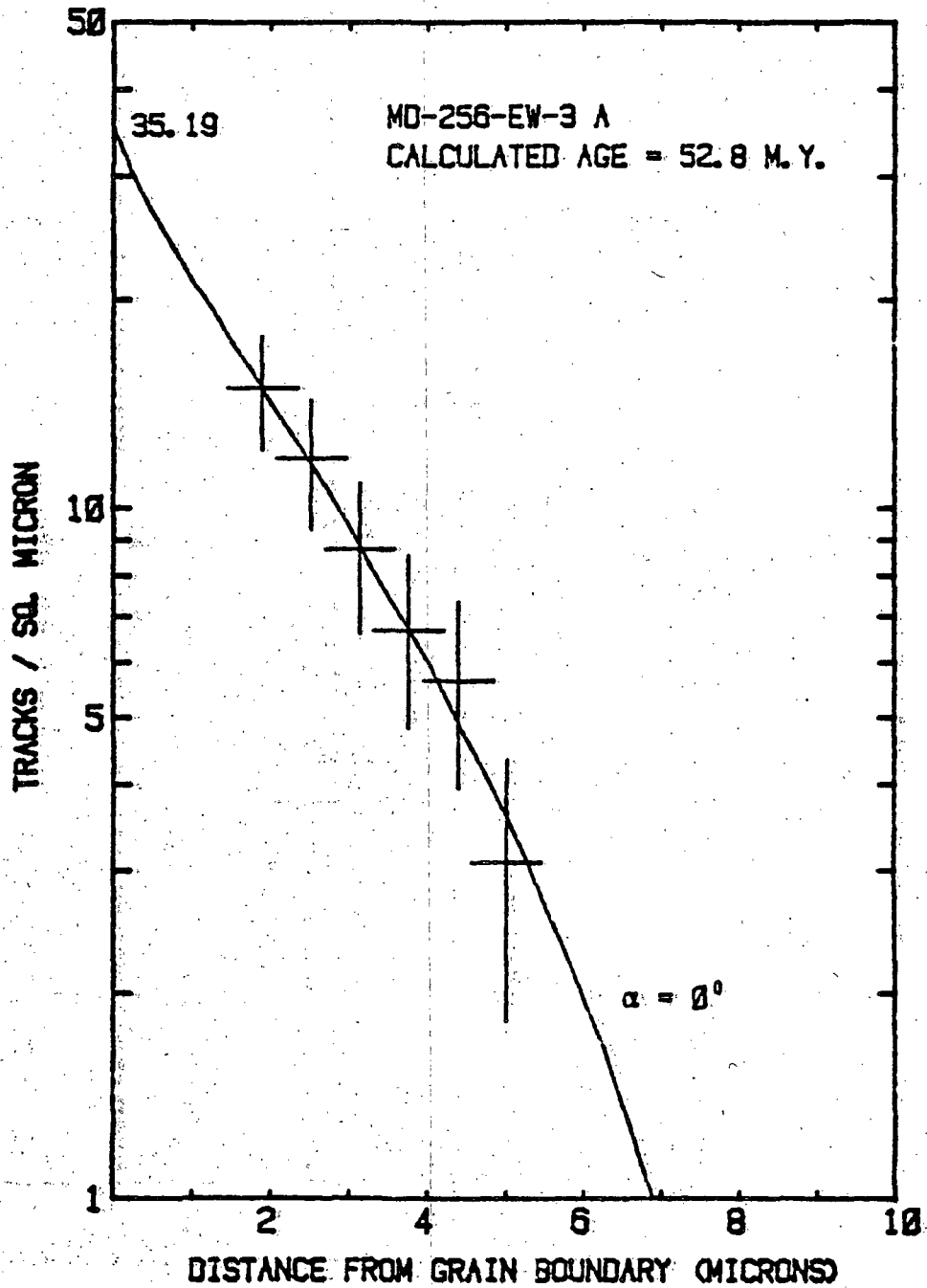* believed to have an uncertainty of ± 10 percent (2σ)

Figure 1. A plot of tracks/μm^2 versus distance from the grain boundary to determine the age of mineralization for the Midnite Mine uranium deposit (Washington); α = grain boundary angle.
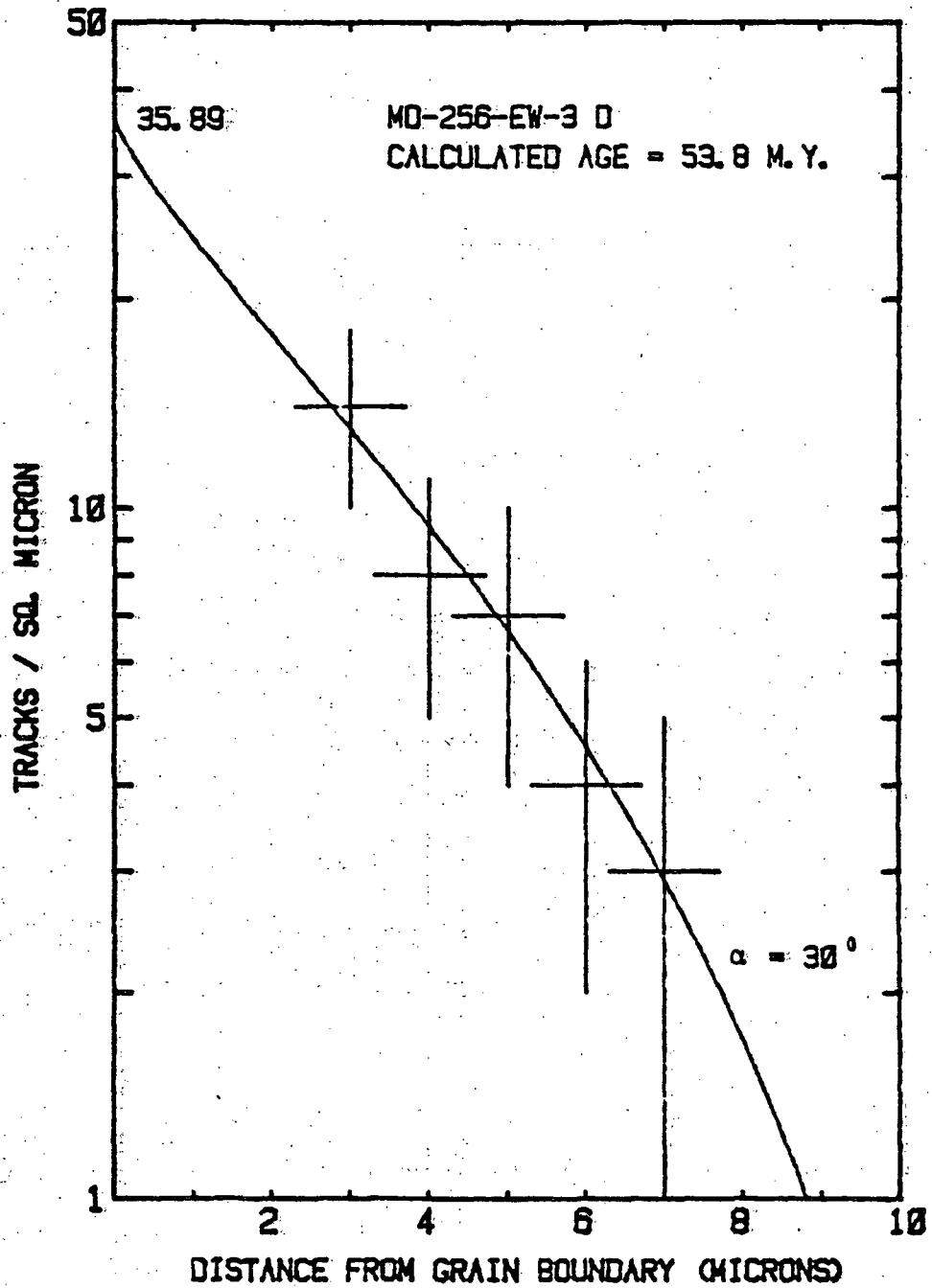
Figure 3. A plot of tracks/μm^2 versus distance from the grain boundary to determine the age of mineralization for the Midnite Mine uranium deposit (Washington); α = grain boundary angle.

through crystal lattices and the fragment's loss of energy over the damage zone must be better understood to obtain accurate track lengths. This is essential for precise numerical evaluation of the theoretical model. The etching efficiency (η^{238}) of the detector mineral is the second area of major concern. Because very few minerals will reveal all the damage zones after etching (Fleischer and others, 1975), determination of the percentage of tracks that will be counted for the number of damage zones actually present is necessary. This will generally change for the various minerals as well as their different cyrstallographic orientations.

For fission track techiques to yield reliable results, the system must have remained closed to loss or gain of U, but not necessarily to the daughter products from the decay of ^{235}U and ^{238}U; quartz must be found adjacent in uraninite or coffinite, with uniform composition of uraninite or coffinite and the correct orientation of quartz desirable; and no thermal event can have occurred where annealing of the damage zones in quartz could have taken place after mineralization.

This fission track dating method should be useful for dating uranium mineralization in an age range of about 10 to 500 m.y., using uraninite adjacent to a quartz detector. This range is based on the expected number of spontaneous fission events naturally occurring in the uraninite, and on the resolution of the etched tracks viewed on the TEM. The method might be extended, however, to older events by use of other U-bearing mineral, such as zircon, sphene, and apatite, where the useful age range will be dependent upon the U-concentration and scale of U-zonation within the mineral chosen.

Ludwig, K. R., Naeser, C. R., and Nash, J. T., 1978, Uranium-lead ages of uranium ores from the Midnite Mine, Washington (abs.) Economic Geology, v. 73, no. 7, p. 1393.

Ludwig, K. R., Szabo, B. J., Granger, H. C., 1977, Pleistocene apparent ores by U-Pb isotope and U-series methods for uranium ore in Dakota Sandstone near Gallup, New Mexico: U.S. Geological Survey, Journal Research, v. 5, no. 6, p. 669-672.

Ludwig, K. R., and Young, E. J., 1975, Absolute age of disseminated uraninite in Wheeler Basin, Grand County, Colorado: U. S. Geological Survey, Journal Research v. 3, no. 6, p. 747-751.

Naeser, C. W., 1976, Fission track dating: U.S. Geological Survey Open-File Report 76-190, 66 p.

Protter, M. H., and Morrey, C. B., Jr., 1964, College calculus with analytic geometry: Palo Alto, Addison-Wesley, 527 p.

Sowinski, M., Stéphan, C., Czyzewski, T., and Tys, J., 1972, Le quartz cristallin detecteur de traces de particules lourdes chargées: Nuclear Instruments and Methods, no. 105, p. 317-322, (in French).
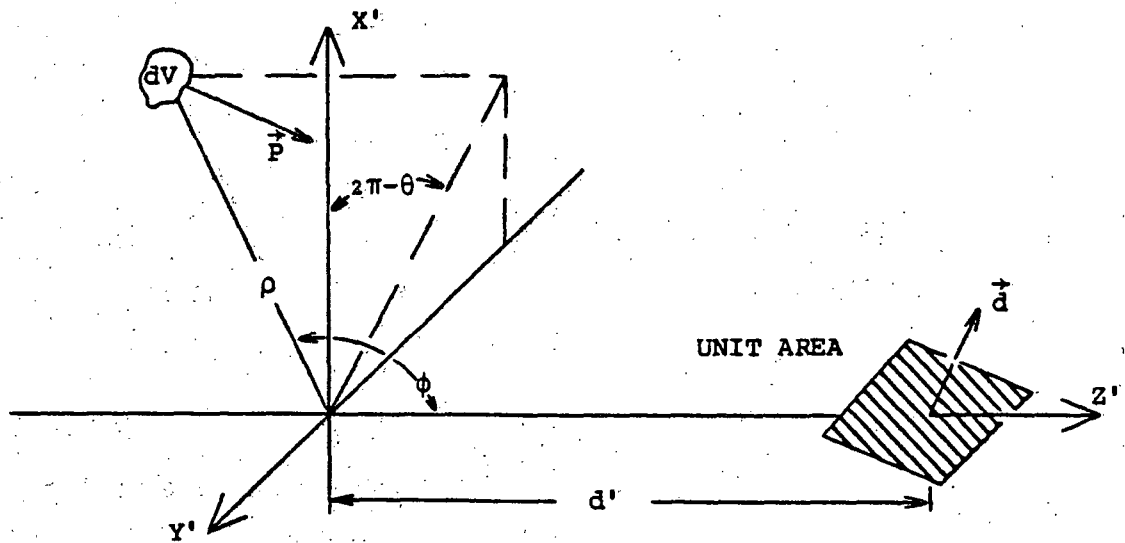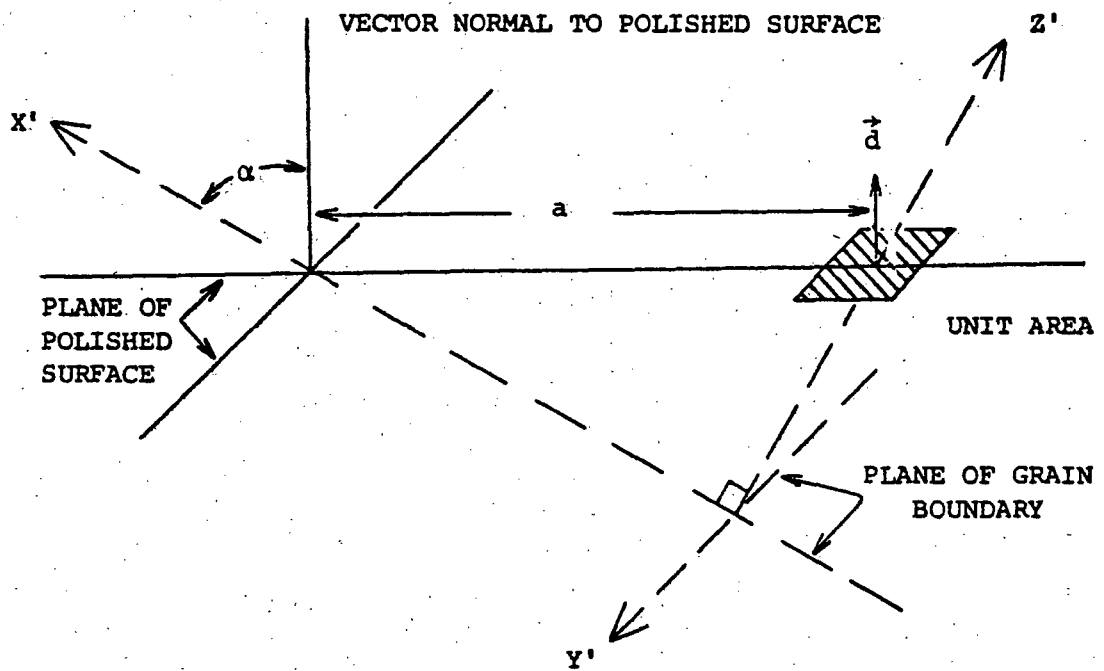
Figure A-1. The geometrical relationships and requisite parameters for setting up the theoretical model are illustrated in these diagrams.
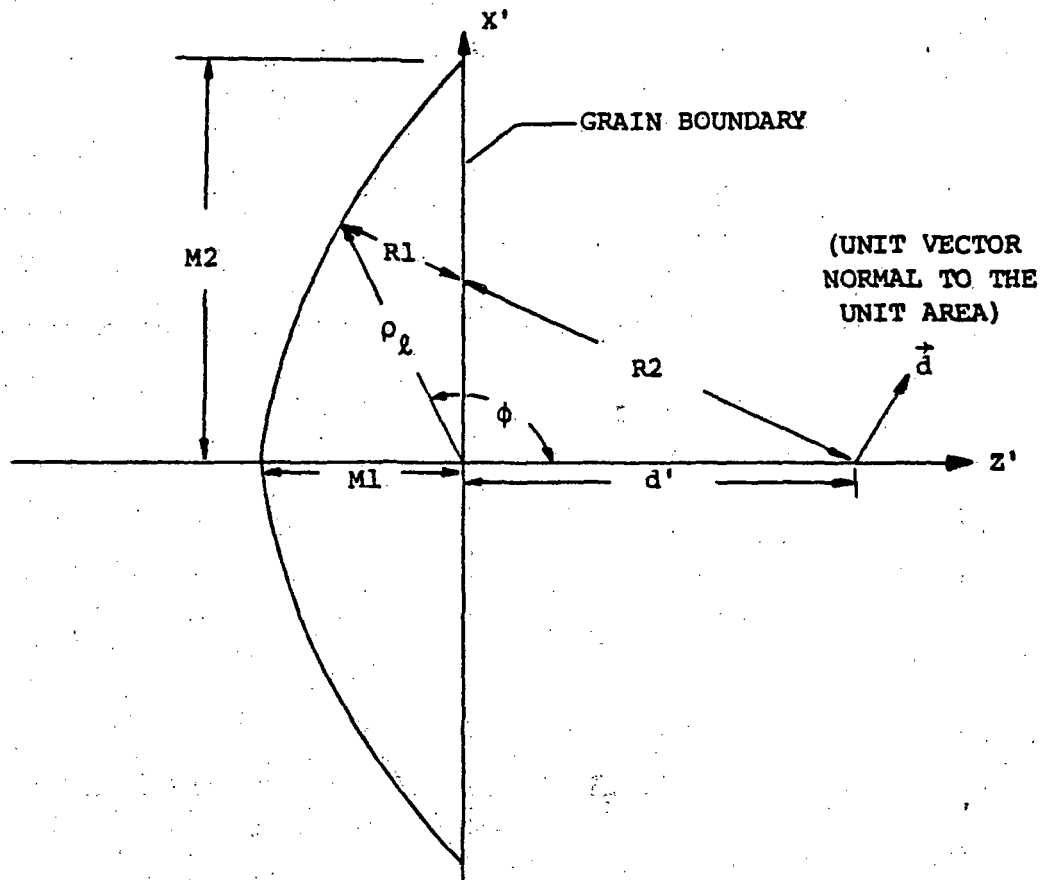
Figure A-2. Two dimensional diagram illustrating quantities required to determine the upper limit for the ρ integration.

therefore dependent upon the angle ϕ but not on the angle θ, again due to the semi-spherical shape (Figure A-2). The total energy loss $\int (dE/dD)$ of the fission fragment will be equal to the sum of the energy loss in phases "a" and "b",

$$\int \frac{dE}{dD} = \left[\frac{dE}{dD} \right]_a + \left[\frac{dE}{dD} \right]_b$$

by conservation of energy. Because the energy loss in each mineral is directly proportional to the distance traveled in that mineral, if this loss is assumed to be a linear relationship, then the sum of the ratios of the distance traveled (R) to the maximum track length (M) is each mineral will be equal to unity for total fragment travel. The energy loss is not actually a linear function of the distance traveled (Friedlander and others, 1964), but the assumption will allow a first order approximation of fragment travel distance especially in materials where energy loss curves are not available. Therefore, the fragment will reach the unit area if:

$$\frac{Ra}{Ma} + \frac{Rb}{Mb} \geqq 1 .$$

This integral is not easily solved exactly due to the absolute value within the numerator and must therefore be solved numerically, using an approach involving Simpson's approximation. Simpson's rule states:

"Suppose that $f(x)$ is continuous for $a \leq x \leq b$ and $\{a = x_0 < x_1 < x_2 < \cdots < x_{2n-1} < x_{2n} = b\}$ is a sub-division of $[a,b]$ into $2n$ intervals of length $h = (b-a)/2n$. Then, approximately

$$\int_a^b f(x) \, dx = \frac{h}{3} \left[f(x_0) + 4f(x_1) + 2f(x_2) + \cdots + 4f(x_{2n-1}) + f(x_{2n}) \right] \text{"}$$

(from Protter and Morrey, 1967).

The computation is further complicated since the maximum distance a fission fragment may travel within a crystal lattice varies from mineral to mineral. Figure A-3 and Table A-1 show presently available data on track lengths for several materials. Thus $\rho\ell$ must be determined during numerical integration as described earlier. Figure A-4 shows the computer program, and table A-3 list the tabulated values from the numerical evaluation of the integral.

TABLE A-1

The average distance a fission fragment will travel in various materials.

Material	Track Length	Reference
Air (STP)	17.0 cm	Friedlander and others, 1964
	15.0 cm	Chadderton & Torrens, 1969
Quartz	10.0 μm	Weiland experimental data
Apatite	8.0 μm	Naeser, oral comm., 1978
$MgSiO_3$	10.0 μm	Schreurs, unpub. data, 1969
$FeSiO_3$	8.5 μm	Schreurs, unpub. data, 1969
MgS_2	5.8 μm	Schreurs, unpub. data, 1969
PbS	3.3 μm	Schreurs, unpub. data, 1969
Ni (metal)	2.8 μm	Friedlander and others, 1964 (Figure 4-6)
Au (metal)	2.5 μm	Friedlander and others, 1964 (Figure 4-6)
U (metal)	3.0 μm	Carpenter, oral comm., 1979
	2.8 μm	Chadderton & Torrens, 1969
UO_2	3.0 μm	Reimer, oral comm., 1979

TABLE A-3

Values of P_r from the numerical evaluation of the theoretical model. The P_r integral was evaluated using Simpson's Rule with a step size ($2n$) equal to 22. These values are for an average maximum fission fragment travel of 3 microns in uraninite and 10 microns in quartz.

Distance from Grain Boundary to Unit Area (microns)	Angle from the Grain Boundary to the Perpendicular of the Polished Surface						
	0°	10°	20°	30°	40°	50°	60°
0.0	1.56	1.56	1.56	1.56	1.56	1.56	1.56
0.5	1.18	1.19	1.22	1.25	1.30	1.35	1.41
1.0	0.942	0.962	1.00	1.05	1.13	1.21	1.30
1.5	0.769	0.787	0.831	0.899	0.991	1.10	1.21
2.0	0.627	0.649	0.693	0.772	0.874	0.990	1.13
2.5	0.513	0.530	0.579	0.659	0.773	0.902	1.05
3.0	0.415	0.430	0.482	0.565	0.685	0.822	0.985
3.5	0.330	0.349	0.399	0.484	0.599	0.746	0.922
4.0	0.266	0.281	0.329	0.408	0.527	0.646	0.861
4.5	0.205	0.222	0.267	0.346	0.462	0.619	0.805
5.0	0.159	0.172	0.216	0.289	0.402	0.558	0.751
5.5	0.118	0.131	0.170	0.239	0.350	0.498	0.700
6.0	0.087	0.098	0.133	0.198	0.302	0.449	0.649
6.5	0.060	0.070	0.101	0.159	0.256	0.401	0.602
7.0	0.041	0.049	0.074	0.127	0.219	0.357	0.600
7.5	0.026	0.032	0.054	0.098	0.184	0.315	0.517
8.0	0.014	0.019	0.036	0.074	0.149	0.276	0.474
8.5	0.007	0.010	0.023	0.054	0.122	0.241	0.437
9.0	0.003	0.005	0.013	0.037	0.097	0.207	0.401
9.5		0.001	0.006	0.025	0.074	0.178	0.363
10.0			0.002	0.014	0.055	0.150	0.330
10.5				0.007	0.039	0.124	0.299
11.0				0.002	0.025	0.101	0.269
11.5					0.015	0.081	0.240
12.0					0.007	0.062	0.212
12.5					0.002	0.046	0.186
13.0						0.032	0.162
13.5						0.021	0.140
14.0						0.012	0.119
14.5						0.006	0.101
15.0						0.002	0.083
15.5							0.068
16.0							0.054
16.5							0.041
17.0							0.031
17.5							0.021
18.0							0.014
18.5							0.008
19.0							0.004
19.5							0.001

```
610 H3=R0/(2*N)
620 REM LOOP TO EVALUATE THE THETA INTEGRATION
630 K6=1
640 MAT Y=ZER
650 FOR T=0 TO (2*PI)+H1 STEP H1
660 T1=SINT
670 T2=COST
680 REM LOOP TO EVALUATE THE RHO INTEGRATION
690 IF R0=0 THEN 950
700 H3=R0/(2*N)
710 K5=1
720 MAT Z=ZER
730 FOR R=0 TO R0+H3 STEP H3
740 F=R^2*P1*(ABS(A1*(D1-R*P2)-R*P1*T2*A2))
750 G=(SQR(D1^2+R^2-2*D1*R*P2))^3
760 Z(K5)=F/G
770 K5=K5+1
780 NEXT R
790 REM EVALUATE SIMPSON'S APPROXIMATION FOR RHO INTEGRATION
800 Y(K6)=FNAN
810 K5=K5+1
820 NEXT T
830 REM EVALUATE SIMPSON'S APPROXIMATION FOR THETA INTEGRATION
840 X(K7)=FNBN
850 K7=K7+1
860 NEXT P
870 REM EVALUATE SIMPSON'S APPROXIMATION FOR PHI INTEGRATION
880 S(J)=FNCN
890 T(J)=D
900 REM PRINT NUMERICAL VALUE OF THE PROBABILITY FUNCTION FOR
910 REM THIS DISTANCE FROM THE GRAIN BOUNDARY AND PROCEED TO NEXT DISTANCE
920 PRINT TAB6,T(J),TAB25,S(J)
930 D=D+DD
940 NEXT J
950 REM INPUT WHERE DATA IS TO BE STORED
960 DISP "STOREDATA IN TRACK#, FILE#";
970 INPUT F1,F
980 STORE DATA #F1,F
990 DISP "DO YOU WISH TO INPUT NEW DATA";
1000 INPUT O
1010 IF O=1 THEN 80
1020 END
1030 REM SUBROUTINE TO EVALUATE SIMPSON'S APPROXIMATION FOR RHO INTEGRATION
1040 DEF FNA(N)
1050 L=M=0
1060 FOR K=2 TO 2*N STEP 2
1070 L=Z(K)+L
1080 IF K=2*N THEN 1100
1090 M=Z(K+1)+M
1100 NEXT K
1110 RETURN H3/3*(Z(1)+4*L+2*M+Z(2*N+1))
1120 REM SUBROUTINE TO EVALUATE SIMPSON'S APPROXIMATION FOR THETA INTEGRATION
1130 DEF FNB(N)
1140 L=M=0
1150 FOR K=2 TO 2*N STEP 2
1160 L=Y(K)+L
1170 IF K=2*N THEN 1190
1180 M=Y(K+1)+M
1190 NEXT K
1200 RETURN H2/3*(Y(1)+4*L+2*M+Y(2*N+1))
1210 REM SUBROUTINE TO EVALUATE SIMPSON'S APPROXIMATION FOR PHI INTEGRATION
1220 DEF FNC(N)
1230 L=M=0
1240 FOR K=2 TO 2*N STEP 2
1250 L=X(K)+L
1260 IF K=2*N THEN 1280
1270 M=X(K+1)+M
1280 NEXT K
1290 RETURN H1/3*(X(1)+4*L+2*M+X(2*N+1))
1300 END
```
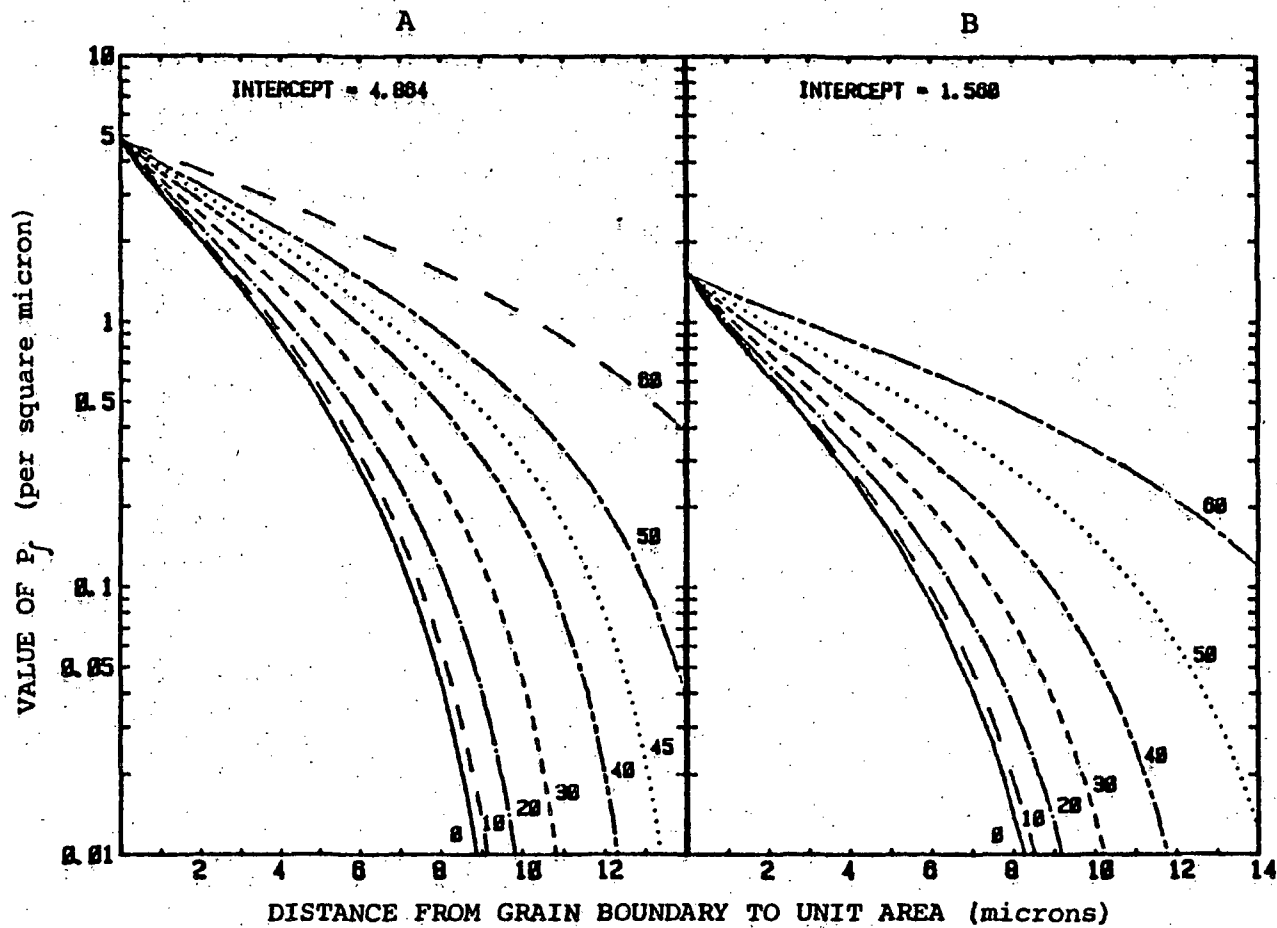
Figure A-5. Theoretical curves determined from the numerical evalua-
tion of the P_f integral for the various grain boundary angles (degrees).
A represents the case where the average fission fragment travel distance
is 10 microns in both the U-rich and U-poor phases, whereas B illustrates
the case where the travel distance is 3 microns in the U-rich phase and
10 microns in the U-poor phase.

252 Cf IRRADIATED QUARTZ SAMPLES

A ^{252}Cf source was used to induce fission tracks in quartz to better understand its etching characteristics. One experiment was carried out to determine etching efficiencies for various crystallographic orientations, while the other experiment measured track lengths and track diameters as a function of etching time.

Etching Efficiency for Quartz

Etching efficiency (η) is defined as

> "the fraction of tracks intersecting a given surface that are etched on the surface under specified conditions" (Fleischer and others, 1975, p. 58).

Since the η^{238} has been established at ~1 for a mica detector (C. W. Naeser oral commun., 1977), the number of tracks etched in the oriented quartz samples were compared to the number of tracks etched in mica detectors irradiated on the same ^{252}Cf source.

Sample Preparation

A large single quartz crystal was slabbed paralled to represented crystal faces (Figure B-1). Several slabs were also cut perpendicular to the C-axis from the remaining crystal core. The slabs were then mounted on glass slide and polished on a vibro-lap unit with tin oxide for 8 hours. This polishing method reduced the problem of crowning found when hand polished on a diamond wheel.

Sample Irradiation

The polished quartz slabs where then placed in direct contact with a ^{252}Cf source (electroplated onto gold foil) for 24 hours. Three mica detectors were placed on the same ^{252}Cf source, again for 24 hours, during the course of this experiment to determine heterogeneity within the source and for calculation of the etching efficiency for quartz.

Sample Etching

The fission tracks in the quartz were then revealed by chemical etching with a 1$\underline{N}$ equimolar solution of NaOH and KOH at $145^{\circ}C$. Etchants previously used for quartz have been described by Fleischer and Price (1964), Sowinski and others, (1972), and Fleischer and others, (1975) with the general conclusion that these etchants are less than satisfactory. Many attempts with HF and $HClO_4$ at several temperatures and concentrations, and various temperatures of NaOH solution were undertaken before the above etchant was decided upon for use in these experiments. The etching apparatus is shown in Figure B-2. The etchant is used until the $145^{\circ}C$ temperature can no longer be maintained, suggesting changes in composition and concentration of the solution. The mica detectors were etched in 48% HF for 14 minutes at $25^{\circ}C$.

Track Counts

Each of the quartz samples were etched for several different time periods, counting between each additional etching. Because of the heterogeneity of the ^{252}Cf source, tracks in the mica detector (sample no. CF-8-23-78-MC) were counted with an optical microscope on a grid system to determine the best areas to use in counting the quartz samples. From this, an area of 25 fields of view, where 1 field of view $= 8.4 \times 10^{-4} cm^2$, centered over the distribution of fission tracks, has been used for all subsequent track counts (Figure B-3).

Results

The results for the different crystallographic orientations are found in Table B-1 and Figures B-4 through B-6. It can be seen that etching efficiency varies considerably for the different orientations. The orientation perpendicular to the C-axis is easily recognized in polished thin sections and shows a generally consistent, but low etching efficiency of 0.38 (Figure

AREA CONTAINING INDUCED
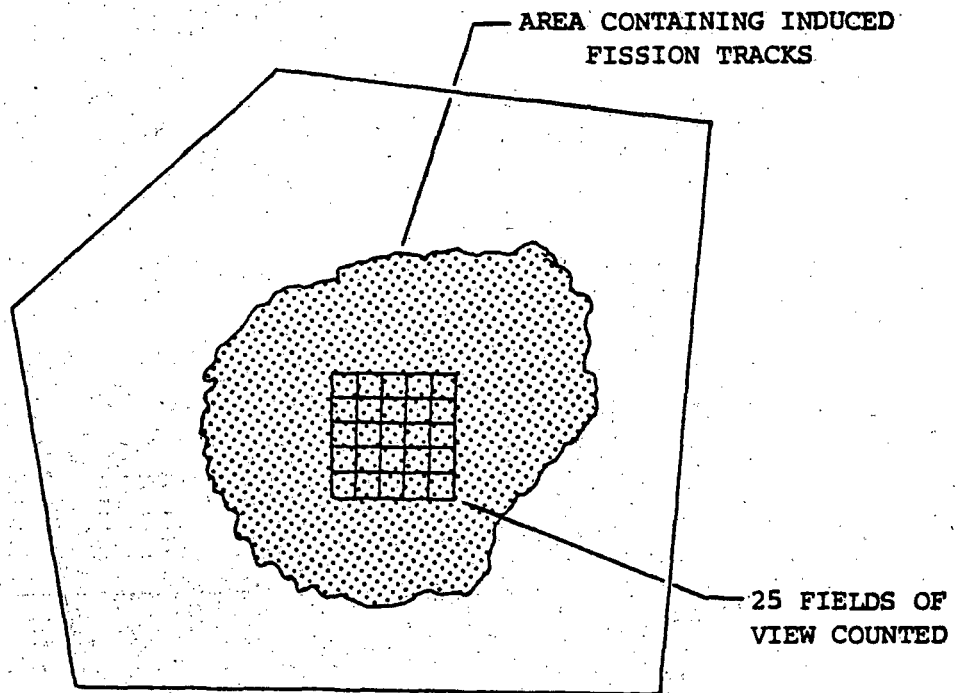FISSION TRACKS

25 FIELDS OF
VIEW COUNTED

Figure B-3. Schematic diagram illustrating area
counted to determine average track density in the
oriented quartz crystals for the experiment on
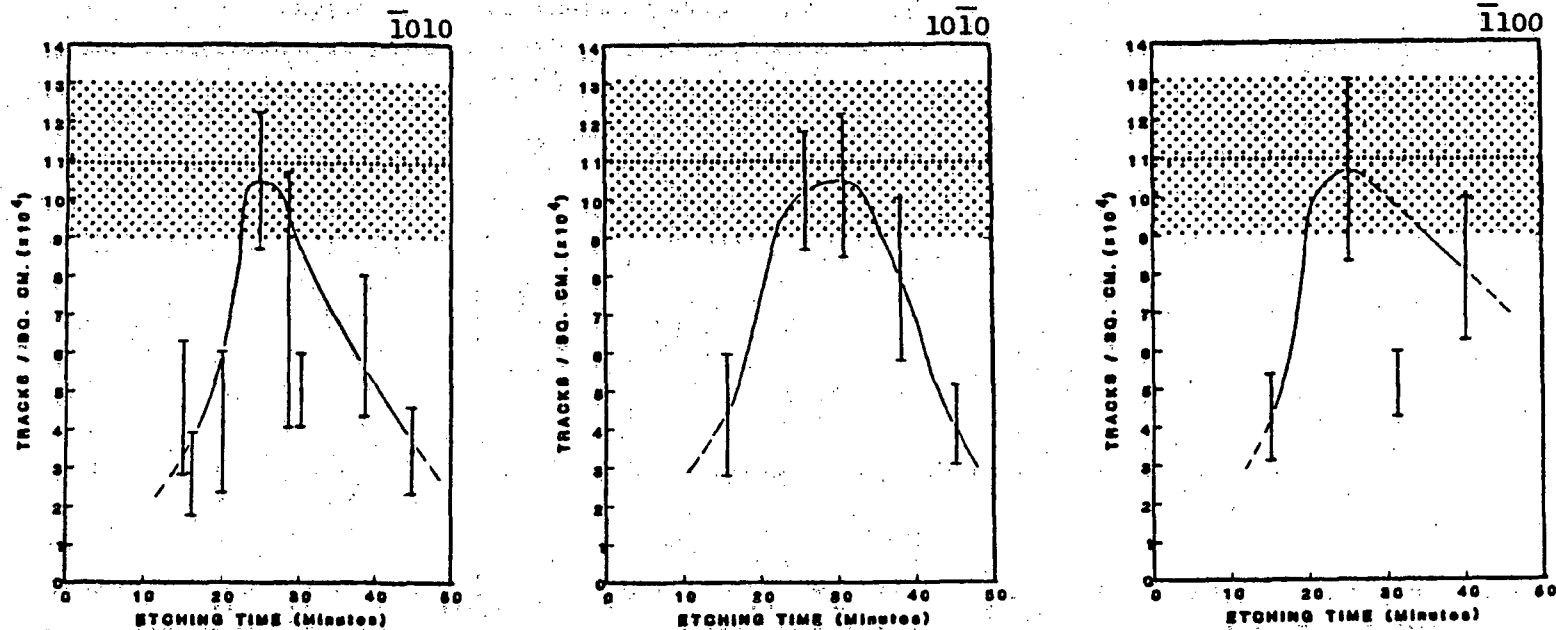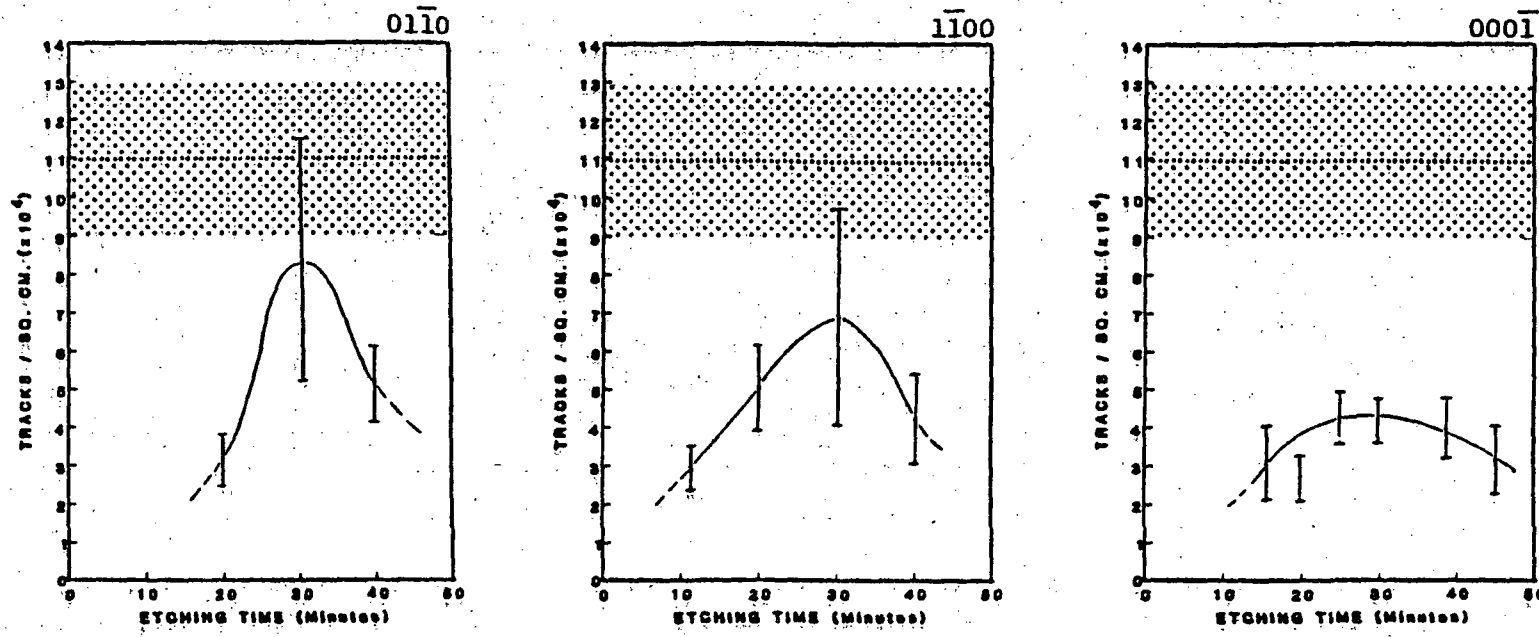etching characteristics.

Figure B-4. Plots of track density versus etching time for data from the ^{252}Cf irradiated quartz samples to determine etching efficiency of quartz relative to mica standards for indicated crystal faces. The stippled bands represent the track density found in mica standards (11 ± 2 x 10^4 tracks/ cm^2).

Figure B-6. Plots of track density versus etching time for data from the ^{252}Cf irradiated quartz samples to determine etching efficiency of quartz relative to mica standards for indicated crystal faces. The stippled bands represent the track density found in mica standards ($11 \pm 2 \times 10^4$ tracks/ cm^2).

FORMVAR SQUARE

ACETONE DROPLET

ETCHED QUARTZ SAMPLE

FORMVAR REPLICA

ETCHED QUARTZ SAMPLE
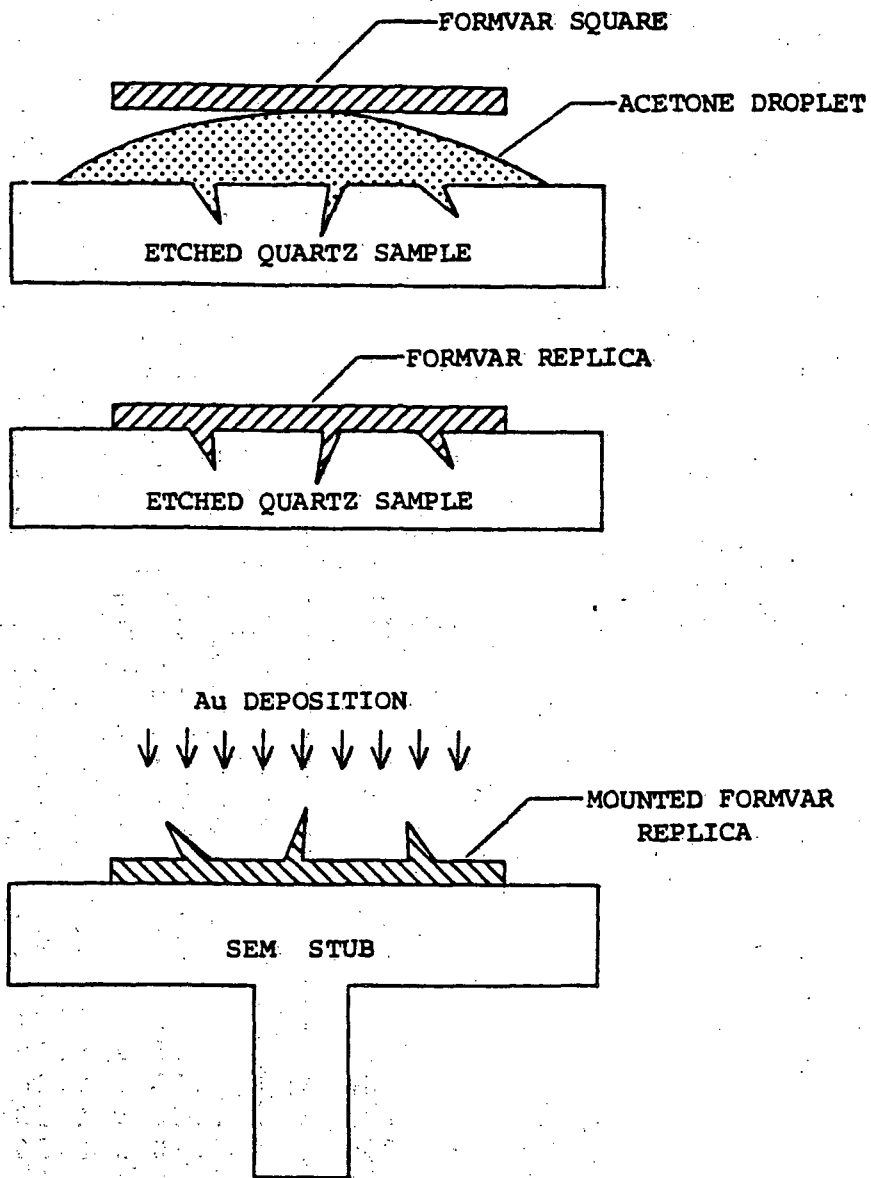
Au DEPOSITION

MOUNTED FORMVAR
REPLICA

SEM STUB

Figure B-7. Replication of etched sample surface
using acetone-softened Formvar (cellulose acetate),
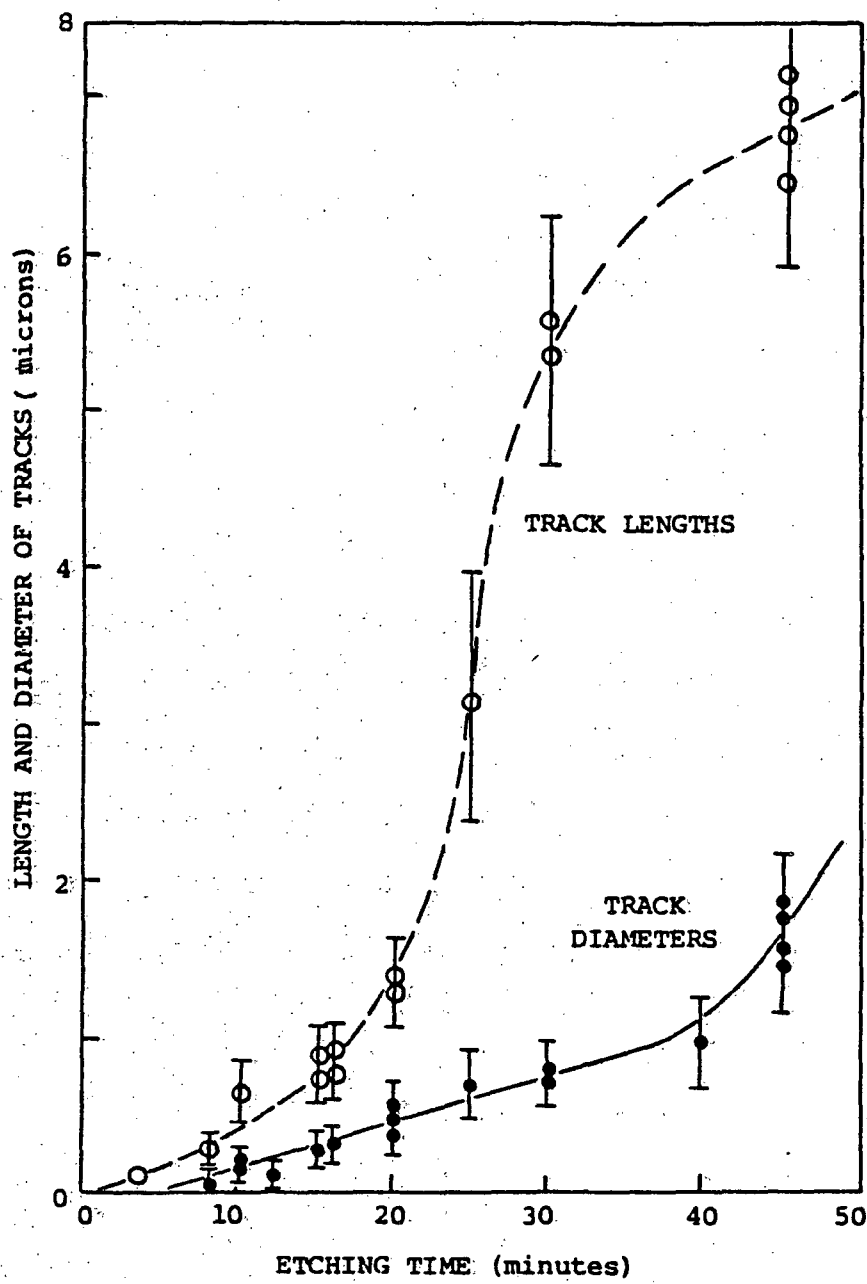and subsequent mounting and coating for observa-
tion in SEM.

Figure B- 8.   A plot illustrating etching time
versus track length and track diameter from
quartz etching studies.

Mounting, Polishing and Etching Grain Mounts

The grains were then mounted using the method described by Naeser (1976):
5-15 grains were placed on a teflon sheet, and several drops of epoxy added to
the grains a glass slide marked with sample numbers was placed on top, using
spacers to level the glass slide (Figure B-9), and the epoxy was allowed to
harden. The grain mounts were polished using the procedure described by
Naeser (1976): Coarse emery paper was used to expose an interior surface of
the quartz grains; and the samples were then unidirectionally polished,
alternating 90° with each decreasing abrasive to the final abrasive of one
micron diamond paste. This polishing procedure allows scratch marks to be
distinguished from fission tracks.

The fission tracks were revealed by the chemical etching procedure
described in the previous section.

Observation and Counting of Tracks

Observation and counting of tracks was accomplished using a scanning
electron microscope (SEM) after the samples had been mounted on a conductive
SEM stub and coated as described in the previous section. Due to inherent
problems with the SEM's operation, the inability to "see into" the etched
track is a major disadvantage of using this machine. Discrimination between
crystal defects, polish scratches, and fission tracks may therefore be
difficult, if not impossible. Resolution of the SEM also limits its use to
track densities generally less than 10^6 tracks/cm^2.

Replication of etched surface as described in the previous section
eliminates most of these problems, but heat from the electron beam tends to
destroy the replica causing a problem with obtaining accurate track
densities. Therefore, for natural samples where track densities are expected
to be greater than 10^9 tracks/cm^2, procedures for the transmission

electron microscope (TEM) were also developed using these irradiated quartz samples.

TEM Specimen Preparation

Since the electron beam must pass through the specimen viewed, the TEM requires a two stage replicating procedure to observe the fission tracks. To make a two stage replica, first the sample is replicated with cellulose acetate as previously described for the SEM, then this plastic replica is taped, replicated side upwards, to a glass slide. This is placed into an evaporative coating system. First, 20-50 $\overset{o}{A}$ of metal (Pd or Pf) is shadow coated at an angle of 20-30^0 from the horizontal (Figure B-10). The formula for calculation of evaporaive coating thickness is:

$$t = \frac{m\ (3\ \sin\ \varepsilon)\ (10^8)}{16\ \pi\ r^2\ d}$$

where

m = mass of material (g)

t = thickness of deposit (A)

ε = shadowing angle (radians)

r = distance from source to specimen (cm)

d = density of material (g/cm^2)

(Kay, 1965)

This coating increases the contrast of the final TEM specimen. Next, a 200-400 $\overset{o}{A}$ carbon coating is evaporated uniformly onto the sample surface. The plastic replica is then dissolved leaving only the metal-carbon replica. The plastic replica is dissolved using methyl acetate by transferring the replica through four such solutions to remove all the plastic residue from the metal-carbon replica. This replica must then be "fished" onto a 100 or 200 mesh copper TEM grid and dried.

TEM Observation and Counting

Photomicrographs of the grains show the etched tracks as light-colored spikes. It can be seen also from the photomicrographs that indicate track densities do indeed decrease with distance from the grain boundary. Track densities computed from the photomosaics at several distances from the grain boundary are shown in Table B-3. Since fission events follow a Poisson distribution (Naeser, 1976), where the standard deviation is the square root of the number of tracks counted, the track density counts were pooled, where possible, to improve the statistics.

Results

Results from these experimental quartz grains are plotted in Figures B-11 and B-12. The intercepts of 18.4, 18.5, and 19.3 tracks/μm^2 show excellent agreement with the calculated track density of 19.7 $\pm$ 2 tracks/μm^2 from the reactor irradiation. Data shown in Figures B-12 from sample #9-12-4FC show no correlation with any of the theoretical curves, and the sharp drop in track density at a distance of 6 microns indicates that this sample may have had another quartz grain in very close proximity when irradiated, yielding the misleading results.

Another noteworthy observation concerns the decrease in track density for distances of less than 2 microns from the grain boundary. This is due to the increased relative etching rate at the corner of a crystal, which is being etched from two surfaces instead of one. This increased bulk etching rate is nearly equal to or greater than the track etching rate, causing the reduction in size and number of tracks at the grain boundary. Therefore, for dating natural samples, track densities were only used for distances greater than 2 microns from the grain boundary to minimize this effect.
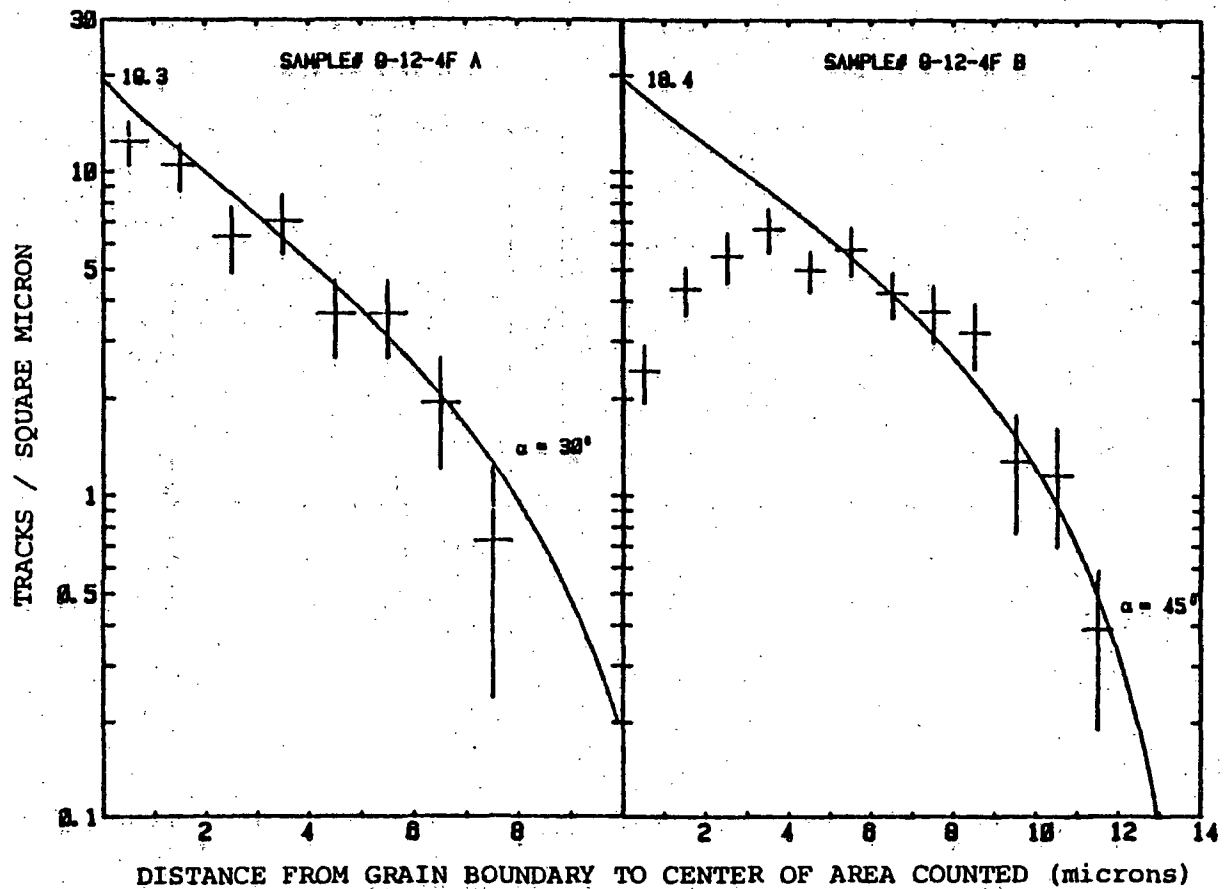
Figure B-11. Plots of track density versus distance from the grain boundary for data from the reactor irradiated quartz samples to test the theoretical model.